Fall 2019

From Experimental Studies to Coarse-Grained Modeling: Characterization of Surface Area to Volume Ratio Effects on the Swelling of Poly (Ethylene Glycol) Dimethacrylate Hydrogels

Gabriel Zahm

FROM EXPERIMENTAL STUDIES TO COARSE-GRAINED MODELING: CHARACTERIZATION OF SURFACE AREA TO VOLUME RATIO EFFECTS ON THE SWELLING OF POLY(ETHYLENE GLYCOL) DIMETHACRYLATE HYDROGELS

by

Gabriel Zahm BS, BA

A Thesis Presented in Partial Fulfillment
of the Requirements of the Degree
Master of Science

November 2019

COLLEGE OF SCIENCE AND ENGINEERING
LOUISIANA TECH UNIVERSITY

LOUISIANA TECH UNIVERSITY

THE GRADUATE SCHOOL

AUGUST 7, 2019
Date

We hereby recommend that the Thesis prepared under our supervision by **Gabriel Zahm**

entitled **From Experimental Studies to Coarse-grained Modeling: Characterization of Surface Area to Volume Effects on the Swelling of PEGDMA Hydrogels**

be accepted in partial fulfillment of the requirements for the Degree of **Master of Science in Biomedical Engineering**

Supervisor of Thesis Research

Head of Department

Department

Recommendation concurred in:

Advisory Committee

Approved:

Director of Graduate Studies

Dean of the College

Approved:

Dean of the Graduate School

ABSTRACT

Understanding the performance of widely applied nanoscale hydrogel biomaterials is an unmet need within the biomedical field. The objective of this master's thesis project was to evaluate the effects size and surface area has on the *in vivo* behavior of nanoscale hydrogels. The hypothesis tested was that at the nanoscale, the increased surface area to volume effects of nanoscale hydrogels play and important role in the overall swelling of hydrogels, such that nanoscale hydrogels swell to a greater degree than their bulk counterparts. To investigate this, the bulk swelling behavior of a series of neutral poly (ethylene glycol) di-methacrylate (PEGDMA) hydrogels was experimentally tested. Along with experimental studies, a computational model based on the experimental findings was developed to serve as a means of predicting nanoscale swelling and subsequent drug release behavior. The computational hydrogel model was validated with the experimental densities and swelling ratios calculated. The surfaces of swollen hydrogels had a density gradient until reaching a stabilized, core density. As the size of the hydrogel decreases, the surface area to volume ratio increases, which enhances surface effects for micro- and nanoscale hydrogels. This conclusion helps to confirm the hypothesis that the increased surface area to volume ratio of nanoscale hydrogels affects the overall swelling ratio in comparison to their bulk counter parts. Particle size should be considered when characterizing nanoscale hydrogels. In this thesis, a computational hydrogel model capable of simulating hydrogel swelling for hydrogels with a dry state

diameter of 40 nm was created. In the future, this model would ideally be able to simulate hydrogels with a dry state diameter ≥ 100 nm to test the full range of nanoscale size effects on hydrogel swelling.

APPROVAL FOR SCHOLARLY DISSEMINATION

The author grants to the Prescott Memorial Library of Louisiana Tech University the right to reproduce, by appropriate methods, upon request, any or all portions of this ThesisThesis. It is understood that "proper request" consists of the agreement, on the part of the requesting party, that said reproduction is for his personal use and that subsequent reproduction will not occur without written approval of the author of this Thesis. Further, any portions of the Thesis used in books, papers, and other works must be appropriately referenced to this Thesis.

Finally, the author of this Thesis reserves the right to publish freely, in the literature, at any time, any or all portions of this Thesis.

Author _____

Date _____

TABLE OF CONTENTS

LIST OF FIGURES

LIST OF TABLES

ACKNOWLEDGMENTS

Firstly, I would like to express my gratitude towards my advisor Dr. Caldorera-Moore, and my co-advisors, Dr. Derosa and Dr. Peters for their support throughout my thesis. I gained invaluable experience from my time at Louisiana Tech University, and I hope I can make a bigger impact on this world because of it. In Dr. Derosa's lab I was presented with all the computational resources required to conduct my research and I am extremely grateful for that. I would like to credit each one of my advisors for the guidance, diligence, patience, and efforts they put in for me to get to where I am today. I thank my lab mates of both Dr. Caldorera-Moore's lab and Dr. Derosa's lab for the valuable insight, help, and comradery. I would also like to thank my family, friends, and loved ones for supporting me in my highs and lows. Lastly, I would like to thank God for being with me every step of the way.

CHAPTER 1

INTRODUCTION

1.1 Hydrogels

1.1.1 An Introduction to Drug Delivery and Hydrogels

Over the past few decades, the ability to precisely control drug release rates for prolonged times has become more and more practical. Despite our increased understanding of the body, drug kinetics, and drug delivery systems, there is still a need for understanding and producing precision medicine for targeted delivery.[1] The objective of controlled delivery is to efficiently and effectively provide therapy to the target site without the use of too little or too much drug. For example, environmentally responsive polymer networks can be triggered by the surrounding environment in the targeted region of the body to release drug therapeutics from the polymer network into the desired area. Controlled drug delivery systems can provide a less toxic route of drug delivery,and allow less frequent dosing, and reduced invasiveness.[2] Ultimately, the ideal drug delivery system should be inert, biocompatible, mechanically strong, non-invasive for the patient, capable of achieving high drug loading, safe from accidental release, simple to administer and remove, and easy to fabricate and sterilize.[2] Although significant progress has been made towards understanding and designing drug delivery systems, there is still plenty of room for growth and optimization in the field. According to the Global Markets and

Technologies for Advanced Drug Delivery Systems, the 2015 market for drug delivery systems (DDS) was around $179 billion with expectations of being around $227 billion by 2020[3].

Hydrogel based systems are commonly studied for drug delivery because of their highly porous structures which are capable of loading and releasing therapeutics[1,4–6]. Such materials have been developed and enhanced for biomedical applications including tissue engineering, regenerative medicine, diagnostics, cellular immobilization, and drug delivery[1,4,7–17]. Hydrogels are three-dimensional, crosslinked polymer networks capable of swelling and retaining large amounts of aqueous solutions in their swollen state, **Figure 1-1**[18,19].

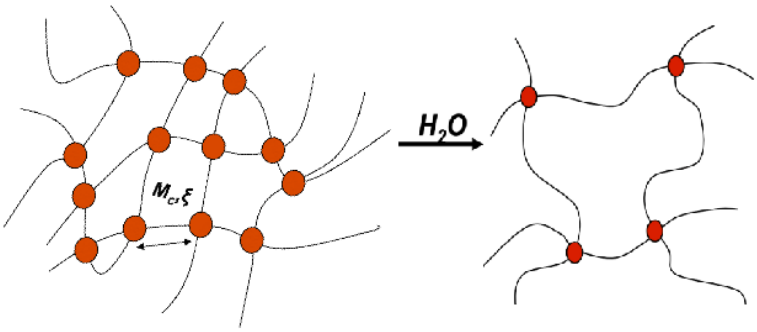

Figure 1-1: A close-up schematic of a crosslinked hydrogel swelling in water[19]

Hydrogels swell through the diffusion of water as a result of capillary, osmotic, and hydration forces, and they are counterbalanced by the elastic force of the crosslinked polymer chains resisting the expansion.[20] Hydrogels can be formed through crosslinking by a chemical reaction between monomers and/or polymers, through physical entanglements through polymer chain interactions, or by a combination of the two[10,20]. In addition to swelling in aqueous solution, hydrogels can be tailored to be stimuli-

responsive and exhibit a volume increase or decrease in response to physical, chemical, or biochemical stimuli such as temperature and pH.[1,4,5,18,21–27] The responsiveness of hydrogels is attributed to the monomers and polymers composing the hydrogel, which can be natural and/or synthetic, and can be anionic, cationic, amphipathic or neutral in charge[10,12,20,25,27–31]. For example, ionic hydrogels have pendant groups attached to the polymer backbone, and upon ionization, the pendant groups will repel or attract each other causing swelling or deswelling. In the same fashion, temperature responsive hydrogels can be developed that can increase or decrease in solubility upon being heated, which drives the swelling or de-swelling of the hydrogels.[4,5,21,27,28,32] Other factors that affect the hydrogel properties and subsequently hydrogel swelling include the molecular weight of the polymer, the concentration of polymer in the hydrogel, the physical size and shape of the hydrogel, and the curing time and energy intensity of thermal or photopolymerization.[27,33] Hydrogels can be developed into a range of physical sizes and shapes, from films and patches to micro- and nano-particulates, based on the desired use[9,24,28]. Bulk hydrogels such as films and patches can be fabricated with relative ease through well-established methods, whereas micro- and nanoscale hydrogel synthesis is more complex but can be done through oil emulsion techniques or photo or imprint lithography.[4,12,21,29,34,35]

Hydrogels are often characterized through swelling studies. These studies are done by putting hydrogels in solvent and allowing them to swell to their maximum extent. The resulting information can be used to provide information about the network's physical properties, including pore size of the resulting hydrogel network and molecular weight between crosslinks.[12,29,30,35] The structural features of hydrogels composed of low

molecular weight polymers whose pores are in the sub-nanometer range are cannot characterized using conventional nanoscale imaging techniques including scanning electron microscopy (SEM), enivironmental SEM, and X-ray computerized tomography. X-ray computerized tomography (μCT) and scanning electron microscopy (SEM) have also been successfully used in imaging, however, the samples studied had macropores[33,36,37]. X-ray computerized tomography works by taking multiple two-dimensional projections, or slices, of a sample, and reconstructing them into a three-dimensional volumetric image[37]. SEM works by creating an image based on the secondary or back scattered electrons interacting with the surface of the sample, which may require a coating of conductive material such as gold, silver, or platinum for better imaging results[36]. Although these techniques can image nanofibers and complex structures, they are not ideal for imaging hydrated samples, and are not able to image hydrogel network pores in the sub-nanometer range.

In summary, hydrogels are highly versatile biomaterials because they can be developed with a controllable initial size (from nanometers to centimeters), shape (patch, capsule, etc), and functionality (pH, temperature, biomolecule responsive), to be suitable for several biomedical applications. Upon tailoring and developing hydrogels, the overall internal structure, surface properties, and maximum water intake of hydrogels can be found through characterization techniques done post-fabrication. The structure of hydrogels can be determined in most cases, however, for nanometer-sized hydrogels, these structural features cannot be accurately characterized.

1.1.2 Characterization of hydrogels

Before controlled drug-release systems could be realized for medical use, a model was developed to simulate diffusion of drug molecules through a membrane. The quantification of drug release into a usable equation known as the Higuchi equation, was originally derived by Takeru Higuchi nearly 60 years ago.[19] The Higuchi equation was able to simplify and address complex drug transport and release from planar devices that opened the window to facilitate device optimization and better understand the underlying drug release mechanisms.[19] The derivation of the Higuchi equation required a number of assumptions that have led to misinterpretations and misuse of the equation, despite favorably contributing to the understanding of controlled drug delivery.[19] Higuchi considered the release of a drug from a thin ointment film into the skin under set conditions in his derivation, which include the following:

1. Drug transport through the ointment base is rate limiting, whereas drug transport within the skin is rapid.
2. The skin acts like a “perfect sink”: The drug concentration in this compartment can be considered to be negligible.
3. The initial drug concentration in the film is much higher than the solubility of the drug in the ointment base.
4. The drug is finely dispersed within the ointment base (the size of the drug particles is much smaller than the thickness of the film).
5. The drug is initially homogeneously distributed throughout the film.
6. The dissolution of drug particles within the ointment base is rapid compared to the diffusion of dissolved drug molecules within the ointment base.

7. The diffusion coefficient of the drug within the ointment base is constant and does not depend on time or the position within the film.
8. Edge effects are negligible: The surface of the ointment film exposed to the skin is large compared to its thickness. The mathematical description of drug diffusion can be restricted to one dimension.
9. The medium (ointment base) does not swell or dissolve during drug release.

Among these considerations, considerations (7) and (8) particularly neglect the surface effects of hydrogels, which are more significant in the nanoscale. Stemming from the Higuchi equation, other theoretical equations came about, which offered a convenient way to categorize controlled release systems: diffusion-controlled, swelling-controlled, and chemically controlled.[19]

The swelling behavior of hydrogels without ionic contributions can be analyzed by the Flory-Rehner theory. The model by Peppas and Merrill has a similar approach to relating experimental values to theory, however, it was made to be applicable to systems where the solvent is present during the crosslinking reaction, as is the case for the hydrogel studied in this thesis.

The idea behind both theories is that a crosslinked polymer gel is subject to two opposing forces: the thermodynamic forces of mixing and the retractive forces of the polymer chains. These forces were related to the free energy of the system, **Eq. 1-1**.

$$\Delta G = \Delta G_{\text{mix}} + \Delta G_{\text{elastic}} \qquad \textbf{Eq. 1-1}$$

Where ΔG is the free energy of the system which can be broken down into the free energy of mixing, ΔG_{mix}, and the elastic-retractive free energy, $\Delta G_{\text{elastic}}$. The full in-depth derivation of the Flory-Rehner theory/Peppas-Merrill equation is described by

Brannon-Peppas and Peppas.[10,12] In summary, the free energy of mixing, ΔG_{mix}, is derived from the entropy change on mixing, ΔS_{mix}, and the heat of mixing, ΔH_{mix}, **Eq. 1-2**.

$$\Delta G_{\text{mix}} = \Delta H_{\text{mix}} - T\Delta S_{\text{mix}} \qquad \textbf{Eq. 1-2}$$

Where the entropy changes on mixing, ΔS_{mix} and temperature, *T*, are subtracted from the heat of mixing, ΔH_{mix}. The elastic contribution of the polymers making up the hydrogel polymer matrix is derived from the statistical theory of rubber elasticity, **Eq. 1-3**.

$$\Delta G_{\text{elastic}} = \frac{kTv_e}{2}(3\alpha_s^2 - 3 - \ln \alpha_s^3) \qquad \textbf{Eq. 1-3}$$

Where v_e is the effective number of chains in the hydrogel network, α_s is the expansion factor of the polymer network, and *T* is the temperature at which the expansion is measured. The differentiation of **Eq. 1-2** with respect to the number of solvent molecules at a constant temperature and pressure, results in the chemical potential of the solvent in a swollen hydrogel, **Eq. 1-4**.[10]

$$\mu_1 - \mu_1^0 = (\Delta\mu_1)_{\text{mix}} + (\Delta\mu_1)_{el} \qquad \textbf{Eq. 1-4}$$

Where μ_1 is the chemical potential of the swelling agent in the polymer-swelling agent mixture, and μ_1^0 is the chemical potential of the pure swelling agent. Using the Flory-Huggins theory, $(\Delta\mu_1)_{\text{mix}}$ can be expressed as **Eq. 1-5**.[21]

$$(\mu_1)_{\text{mix}} = RT[\ln(1 - v_{2,s}) + v_{2,s} + \chi_1 {v_{2,s}}^2] \qquad \textbf{Eq. 1-5}$$

Where $v_{2,s}$ is the polymer volume fraction in the swollen state, *R* is the universal gas constant, and χ_1 is the free energy mixing parameter of polymer and solvent. Using the Flory-Huggins theory, $(\Delta\mu_1)_{el}$ can also be expressed as **Eq. 1-6**,[21]

$$(\Delta\mu_1)_{\text{el}} = RT\left(\frac{V_1}{vM_c}\right)\left(1-\frac{2M_c}{M_n}\right)v_{2,r}\left[\left(\frac{v_{2,s}}{v_{2,r}}\right)^{1/3}-\frac{1}{2}\left(\frac{v_{2,s}}{v_{2,r}}\right)\right] \qquad \textbf{Eq. 1-6}$$

where V_1 is the molar volume of the water, M_n is the number-averaged molecular weight of the unreacted polymer, v is the specific volume of the polymer, $v_{2,r}$ is the polymer volume fraction in the relaxed gel, and M_c is the average molecular weight between crosslinks.

The difference between the Flory-Rehner theory and the Peppas-Merrill equation, **Eq. 1-7**, becomes a matter of when the crosslinks are introduced.

$$\frac{1}{M_c} = \frac{2}{M_n} - \frac{\frac{v}{V_1}\left(\ln\left(1-v_{2,s}\right)+v_{2,s}+\chi_1 v_{2,s}^2\right)}{v_{2,r}\left(\left(\frac{v_{2,s}}{v_{2,r}}\right)^{\frac{1}{3}}-\left(\frac{v_{2,s}}{2v_{2,r}}\right)\right)} \qquad \textbf{Eq. 1-7}$$

For the Peppas-Merrill equation, $v_{2,r}$ considers the initial relaxed state of the hydrogel when the crosslinking occurs. For the original Flory-Rehner theory, **Eq. 1-8**, $v_{2,r}$ is considered to equal 1 and is used for when the hydrogel is crosslinked in the solid state.

$$\frac{1}{M_c} = \frac{2}{M_n} - \frac{\frac{v}{V_1}\left(\ln\left(1-v_{2,s}\right)+v_{2,s}+\chi_1 v_{2,s}^2\right)}{\left[{v_{2,s}}^{\frac{1}{3}}-\frac{v_{2,s}}{2}\right]} \qquad \textbf{Eq. 1-8}$$

The Peppas-Merrill equation uses experimental swelling study values to relate the structure and morphology of the hydrogel material to diffusion.[19] Specifically, the average molecular weight of the polymer chain between two neighboring crosslinking

points (M_c), and the corresponding mesh pore size (ξ), seen in **Figure 1-2**, can be determined.[12]

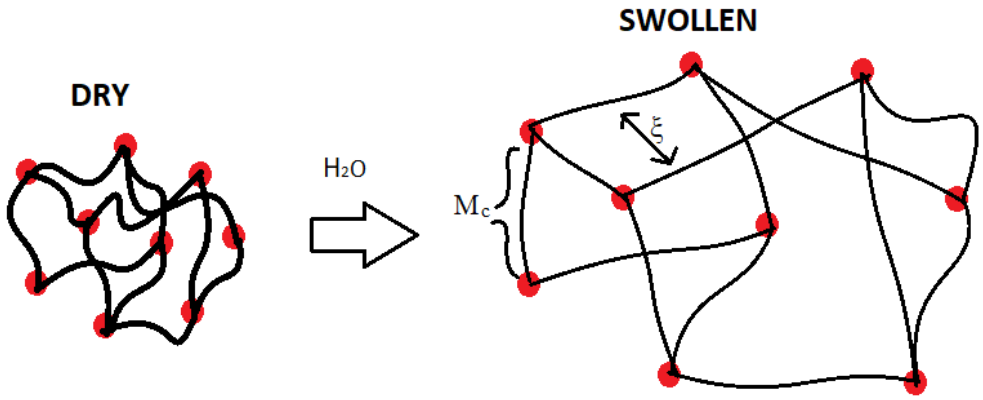

Figure 1-2: Dry and swollen state hydrogels showing the swollen state ξ and M_c parameters. Red beads represent the crosslink points and black lines represent the polymer chain.

The mesh pore size, ξ, is important for determining whether a loaded drug within the hydrogel can be sufficiently transferred to the target site, and can be determined through **Eq. 1-9**, or equivalently, by substitution, as **Eq. 1-10**.[34]

$$\xi = \alpha(r_0{}^2)^{1/2} \qquad \textbf{Eq. 1-9}$$

Where α is the elongation ratio from the hydrogel dry state to the hydrogel swollen state, and $(r_0{}^2)^{1/2}$ is the polymer distance from crosslink to crosslink. The experimental pore size calculation can be determined by substitution seen in **Eq. 1-9**.[34]

$$\xi = v_{2,s}{}^{-1/3}\left(\frac{2C_nM_c}{M_r}\right)^{1/2} l \qquad \textbf{Eq. 1-10}$$

In the substitution, α is equivalent to $v_{2,s}{}^{-1/3}$ and $(r_0{}^2)^{1/2}$ is substituted with $\left(\frac{2C_nM_c}{M_r}\right)^{1/2} l$. C_n is the characteristic ratio of the polymer, M_r is the molecular weight of the monomer

repeat unit, and l is the average bond length of the atoms composing the monomer. With these outputs, the physical properties of the hydrogels can be understood and be modified and used for specific applications. For instance, therapeutic agents of a given size will not be released from a network whose pores are smaller than the therapeutic agent until the pores swell to be large enough to fit it. The pore size calculation would then be useful in determining the best hydrogel formulation for therapeutic agent release.

Within the Peppas-Merrill equation, assumptions are made to simplify the network and its characterization. For bulk hydrogels, these assumptions may be valid, however, they do not necessarily hold true in the nanoscale. The assumptions include:

1. That the volume change reflected in the elastic portion is assumed to be equal in all 3 dimensions.
2. That the crosslinks are tetrafunctional and fully crosslinked.[5,38]
3. That the density of polymer and crosslinks throughout the hydrogel is uniform, such that there are no differences in entropy, enthalpy, and elasticity, or the overall ΔG based on the distance from the center to the edges of the hydrogel.[27]

The Peppas-Merrill equation has been used with known limitations to characterize the internal crosslinked hydrogel structure using information provided by swelling studies and of the polymer water interactions. Although it is considered to be the gold standard of characterization for nonionic hydrogel systems, the Peppas-Merrill equation does not account for swelling differences observed in nanoscale hydrogels.[10,12,35,39]

Smaller objects of the same shape have a larger surface area to volume ratio than larger counterparts. This surface area to volume ratio is larger and becomes much more relevant at the nanoscale. Factors that differ between near-surface and bulk regions of

hydrogels will affect nanoscale hydrogels more strongly than for the bulk hydrogels. These factors can be surface wetting, density, elastic constraints, degree of entanglement, etc. that are no longer able to be averaged into the "bulk" calculations. A difference in surface density would be a violation of Assumption 3, which would inevitably violate Assumption 1. This dominating size factor was studied by Caldorera-Moore *et al.*, where it was found that the swelling of nanoscale hydrogels is comparable to the bulk when the length of the particle is longer than 400 nm while the width and height were 100 nm[35]. The implementation of a computational model could serve as a predictive model for the swelling behavior of hydrogels within the body and can confirm and evaluate how size and increased surface area affect the swelling of hydrogels since it cannot be directly measured experimentally at the nanoscale. A model would allow for flexibility with the degree of crosslinking and would be more encompassing and accurate when determining the swelling characteristics of different polymer blend hydrogels.

1.1.3 Thesis Approach

In this thesis, poly(ethylene glycol) di-methacrylate, PEGDMA, was used to conduct experimental swelling studies to obtain the initial parameters of the computational model. Poly(ethylene glycol) (PEG) hydrogels have been widely studied and used in drug delivery and biomedical applications because of their functionality, biocompatibility, and stealth properties that allow PEG molecules to reach the target tissue without being attack by the immune system.[6,22,28,32,40–45] These stealth properties are attributed to PEG's inherent repellence to cells.[12] PEG reduces particle aggregation which increases the drug formulation's stability in storage and application, is fairly

inexpensive, and is approved by the FDA, making it an ideal candidate to be studied further for size effects.[6]

PEGDMA is a neutral polymer with UV sensitive, trifunctional terminals (DMA) capable of being chemically crosslinked to form a hydrogel. The molecular weight of PEGDMA can range from the tens to the thousands, and can be crosslinked chemically, through irradiation, or photopolymerization to form the 3-dimensional network.[21] A similar hydrogel, poly(ethylene) glycol diacrylate, has been developed by Caldorera-Moore *et al.*[35] through imprint lithography to fabricate bulk and nanoscale hydrogels, which led to the hypothesis being studied in this thesis. The results showed that there was a significant increase in the degree of swelling for the hydrogels below the 100 nm range compared to their micro- and bulk counterparts[35]. The current models characterizing hydrogel swelling do not account for these differences.

The parameters obtained in the experimental swelling studies along with the parameters from scholarly sources regarding modeling of poly(ethylene glycol) were then used to build an accurate computational model of neutral PEGDMA hydrogels at a range of sizes within the nanoscale. Once the model was built, the hydrogel was simulated to swell in water and be characterized by its dry and swollen state. The overall objective was to create a scalable hydrogel model that had all the same build features so that the effects of size and surface area to volume ratio could be evaluated.

1.2 Computational modeling of polymer networks

1.2.1 Polymer modeling

Flexible polymers like PEG are highly elastic and deformable. These molecules are capable of rotating around the bonds along the backbone and forming coils with an end-to-end distance significantly shorter than their elongated forms, as seen in **Figure 1-3**.

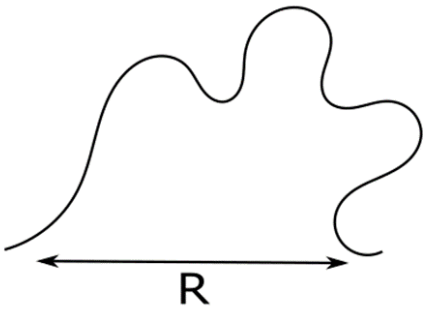

Figure 1-3: Flexible polymer with end-to-end distances shown.

This is reflected in the elasticity of polymers and allows for stretching and uncoiling, however, the forces sustained by the elastomer chains are entropic. The stretched configuration of the chains means fewer available conformations are possible which causes an increase in the network energy. Classical affine theory of elastomer networks assumes Gaussian, freely-jointed chains with the same end-to-end length distribution throughout the network, incompressibility of the network, affine deformation with affine boundary conditions, and the total energy in the network is the sum of the energies of the chains within the network[46,39]. Affine deformation in elastomer networks was previously assumed if the boundaries deformed affinely. Small angle neutron scattering (SANS)

suggests global affine deformation does not necessarily translate to local affine deformation.[47,48] The consensus for non-affine deformation in polymer networks is that interchain effects such as the interchain excluded volume and entanglements cause the non-affine deformities. Closely tied with this supposition is that the local change of crosslink density across a polymer network and the concentration of polymer induce non-affine deformation.[49,50] This discrepancy in deformation comes down to a variance in single chains, which would have a larger effect in smaller samples. Deformation at the surface of the hydrogel, where the polymeric network is less constricted by crosslinks, would differ from the more constricted center. This would likely result in different swelling behavior at the surface of the hydrogel as compared to the core, resulting in different swelling for nanoscale hydrogels as compared to bulk hydrogels. An accurate model representation of a polymer network would entail having localized deformation of polymers and entanglements within a global network representative of a nanoscale hydrogel.

1.2.2 Determining the scale of the computational model

The random nature of polymers within elastomer networks along with entanglements, attractions, and repulsions can make the modeling of elastomer networks complex. At bulk length-scales, reasonable results can be obtained by assuming a normal distribution within a network, while at atomic scales polymer twists and entanglements can be explicitly modeled, but simulation volumes are severely limited. To study effects at the nanoscale, we require a model that accounts for entanglements, but also reaches length scales in the 10's of nm.

Computational modeling exists on many scale lengths from the quantum level of Angstroms (10^{-10} m) to centimeters and meters, as seen in **Figure 1-4**.[51–54]

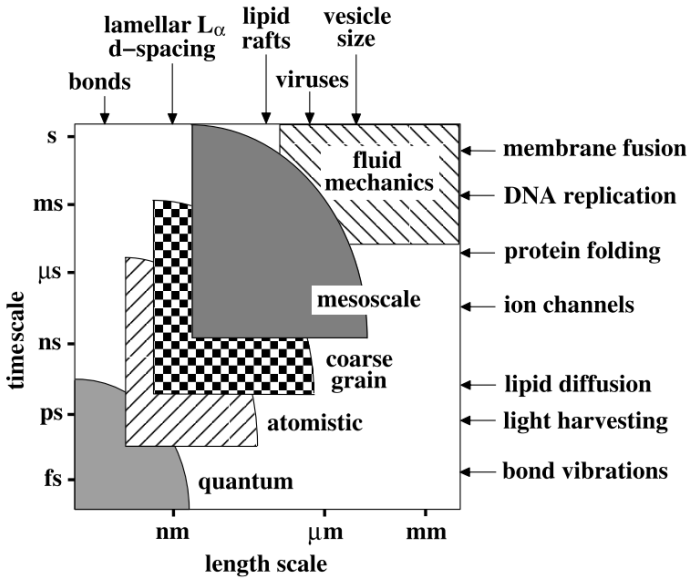

Figure 1-4. A Schematic diagram of temporal and spatial scales accessible by simulation techniques. Also indicated are some characteristic membrane structures and events[55].

The time scale at which these lengths are represented are related to their size and can range from seconds to smaller than femtoseconds (10^{-15} s). The objective of choosing the modeling approach is to find a representative scale length that is accurately determinses the desired characteristics while maintaining the computational efficiency of the model.

In this work, nanoscale hydrogels are being studied particularly for their deformation and swelling observed as they absorb water, with an emphasis on the effects of size on the global swelling of the hydrogel. These size effects are known to play a role in hydrogel swelling, yet no current methods are available to understand how and why they exist. By creating a model, the size and surface area to volume ratio effects can be better understood, and the model itself could serve as a predictive tool to simulate the

swelling process without any experimental contribution. The overall network effects in hydrogel swelling cannot be fully simulated on atomistic scales because of the computational expense of modeling a large enough sample that captures the network topology, the pore sizes, and the physics. On top of the computational expense, the time step for atomistic models must consider bond vibrations, meaning a maximum time step around 10^{-15} s (1 femtosecond). These factors alone, give reason to assess hydrogel swelling on a larger scale. Although coarse-grained dynamics can still be computationally expensive, the time steps can be 20-50 times longer than atomistic capabilities, while also modeling a larger system.[56–58] Coarse-graining allows enough detail to capture the bridge between the chains and the overall network while maintaining the physics associated within. Complex systems can be simulated by simplifying the representation and decreasing the degrees of freedom allowing for longer simulation times.

1.2.3 Coarse-graining

One of the more common ways of coarse-graining is to consider the repeat units as a bead with elastic connections to develop what is known as a bead-spring model.[13,52,58–63] The bead is mapped to preserve structural symmetry that would be compatible with the coarse-grained water model. The structural and dynamic properties can be attained by matching the atomistic references to the coarse-grained system, pictured in **Figure 1-5**.[62,63]

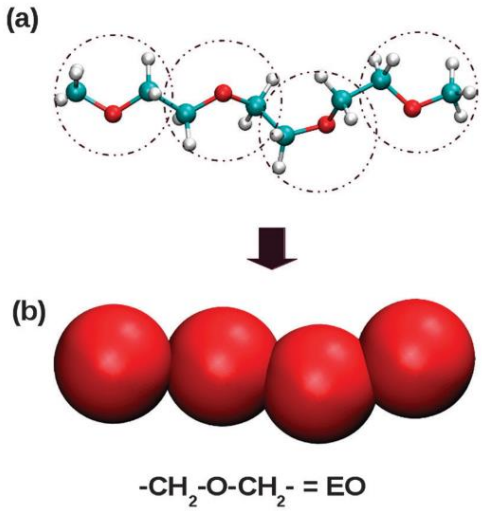

Figure 1-5. Atomistic (a) and coarse-grained (b) representations of poly(ethylene glycol) dimethylether chain (PEG-DME). Each -CH2-O-CH2 repeat unit is mapped into one coarse-grained EO site.[40].

One common way to parameterize the beads is to fit to structural properties such as the radial distribution functions derived by atomistic simulations.[55,56] Other options include matching the average force exhibited on the atom cluster represented by coarse-grained bead.[42,52,56–58,61] Fortunately, poly(ethylene glycol) is a widely studied polymer whose mapping has been extensively studied, and is the polymer repeat unit of PEGDMA that I have chosen to study for my thesis.[6,18,22,28,32,40–45]

The bead-spring model can be effectively applied with two methods, Monte Carlo and molecular dynamics. In the Monte Carlo approach, particles are given a probability of moving individually or as aggregates to a neighboring site which is then accepted or not based on the energy change due to the move and an associated probability[64–66]. The molecular dynamics approach of the bead-spring model is a simulation of the monomer or groups of monomers and their bonds by solving Newton's equations of motion.[15,52,56,67] This method allows for predictive deformation and enables

entanglements to occur, which would allow future kinetic/diffusion studies, which Monte Carlo will not allow. The molecular dynamics approach was taken in the hopes of better characterizing the polymeric network and its use in predictive swelling across all size scales.

In the case of my thesis, a coarse-grained model was built to be able to accurately model networks in the range of 5-25 nanometers in each dimension in the dry state, enough to study the effect of a large range of surface area to volume ratios.

CHAPTER 2

EXPERIMENTAL METHODS

2.1 Experimental Methods

Hydrogel network pore size and molecular weight between crosslinks can be characterized through swelling studies as previously described.[4,12,19,30,33–35,39,68] Although it is not done in this work, knowledge of these swelling characteristics can then be applied towards determining the solute diffusion coefficient, the surface properties and mobility, the optical properties, and mechanical properties.[21] These factors can be essential for understanding drug loading and diffusion through the network among other uses. The following methodology is for the preparation of poly(ethylene glycol) di-methacrylate, PEGDMA, hydrogels. The goal of developing PEGDMA hydrogels and conducting swelling studies was to gather data to be used to accurately create a scalable computational hydrogel model. The hydrogel model would then serve as a predictive model for nanoscale hydrogel swelling capable of isolating the size effects on the overall swelling and structure of hydrogels.

In this study, the molecular weight (MW) of PEGDMA, percent by weight (% wt.) of polymer to water, and UV intensity were varied to investigate the effects each contribution had on the resulting hydrogels' overall swelling and structural features.

PEGDMA is a polymer whose terminals can be photoinitiated to crosslink with other PEGDMA terminals to create a crosslinked hydrogel network. The optimal amount of photo-initiator, the intensity and time required to cure the following sized hydrogel films were predetermined by the lab group through a series of tests and outside research. The two molecular weights of PEGDMA used were of 750 Daltons and 1000 Daltons, acquired from Sigma Aldrich and Polysciences Inc., respectively. The percent by weight of polymer to water was tested at 25, 30, and 50 % wt. Ultimately, 12 different hydrogel formulations were developed, 6 at high intensity (~33 mW/cm^2) and 6 at low intensity (~13 mW/cm^2), as summarized in **Table 2-1.**

Table 2-1: Formulations for varying percent polymer of different molecular weight PEGDMA at low and high intensity, with actual values listed.

% polymer	MW PEGDMA	UV intensity	Polymer (g)	DIH_2O (g)	Photoinitiator I2959 (g)
25	750	LOW	2.515	7.4994	0.0124
		HIGH	2.4987	7.5109	0.01274
	1000	LOW	2.5048	7.4961	0.0128
		HIGH	2.5017	7.5197	0.01254
30	750	LOW	3.0034	7.0423	0.0124
		HIGH	3.014	7.0073	0.0149
	1000	LOW	2.9921	7.0045	0.01532
		HIGH	3.013	7.0114	0.0155
50	750	LOW	5.0155	5.0142	0.02481
		HIGH	5.0138	5.0019	0.0253
	1000	LOW	4.9935	5.0256	0.02558
		HIGH	5.05	5.009	0.0256

2.2 Materials

The materials used in the synthesis and swelling studies of hydrogels can be found in **Table 2-2**.

Table 2-2: List of materials used in the experimental methods with the abbreviations, company they were acquired from, and the identity/purpose of the material.

Materials	Abbreviation	Company	Identity/Purpose
Poly(ethylene glycol) dimethacrylate MW 750	PEGDMA 750	Sigma Aldrich	Polymer with crosslinker terminals
Poly(ethylene glycol) dimethacrylate MW 1000	PEGDMA 1000	Polysciences Inc.	Polymer with crosslinker terminals
Deionized Water	DIH_2O		Solvent for synthesizing hydrogels. Obtained with a Millipore deionization system
2-Hydroxy-4'-(2-hydroxyethoxy)-2-methylpropiophenone	I2959	Sigma Aldrich	Photoinitiator, Lot #: MKBJ9842V
Heptane		Fisher Scientific	Non-solvent used with density kit (0.684 g/cm3)
1X Phosphate Buffered Saline	PBS	Sigma Aldrich	Solvent for swelling hydrogels (pH 7.4, 1X molarity)
Teflon Spacer		Dupont	1 mm thick, separates photomask to control hydrogel thickness
Soda lime photomask			Transparent encasement for hydrogel precursor solution
Biopsy Punches		Fisher Scientific	Cuts circular discs of 1.5 cm diameters from hydrogel film

The equipment used for the synthesis and swelling studies of hydrogels can be found in **Table 2-3**.

Table 2-3: List of equipment used in the experimental methods with the abbreviations, company they were acquired from, and the identity/purpose of the equipment.

Equipment	Company	Identity/Purpose
Ultrasonic Bath	Bransonic Inc.	Sound waves agitate particles in precursor solution. Removes dissolved gas and induces dissolution of solids into liquids
Vortex Mixer	Benchmark Scientific Inc.	Mixes precursor solution (Serial #: 11112183)
Sartorius Scale and Hanging Basket Apparatus	Sartorius Weighing Technology	Measures weight and density using air and heptane weight measurements
Dymax Light Curing Machine	Dymax Light Curing Systems	400 Watt UV light source for crosslinking hydrogels (Serial #: 3001780)
Orbital Shaker Plate	VWR Orbital Shaker	Generates circular shaking motion to rinse hydrogel discs in centrifuge tubes
Vacuum Chamber	Lab-line Instruments	Dries hydrogel discs. Kept at 40°C and 90 kPa

2.3 Hydrogel Synthesis

The precursor solutions were prepared in a labeled 50 ml amber bottle by weighing out the required amount of PEGDMA and DIH_2O, **Table 2-1**, using the Sartorius scale. The solution was then mixed with the vortex mixer for 2 minutes. Photo-initiator, I2959, was then added to the precursor hydrogel solution at a 0.5% wt. with respect to the PEGDMA mass used. Two soda lime photomasks were then placed atop one another with 2 Teflon spacers in-between to achieve a 2 mm thick separation, with clamps to form a seal around the edges, as shown in **Figure 2-1**.

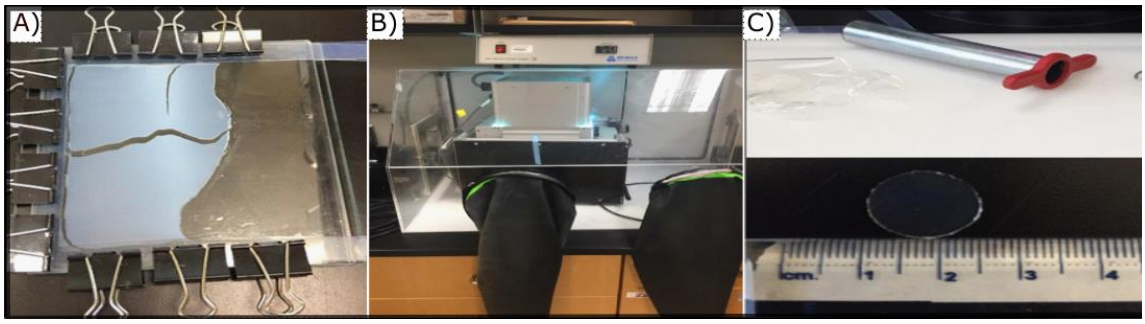

Figure 2-1: A) Sample photomask setup consisting of 2 glass plates, 2 teflon spacers cut to line 3 edges of the plates, and 10 clamps to form a seal. **B)** A Dymax Light Curing machine used to cure hydrogels. **C)** A size 8 disc cutter with a freshly cut hydrogel disc.

The precursor solution was then sonicated in the ultrasonic bath for 20 minutes and was pipetted into the sealed photomask structure, **Figure 2-1-A**, and immediately set to cure in the Dymax Light curing machine, **Figure 2-1-B**, for 5 minutes at 320-390 nm UV-A at either a low intensity range of ~13 mW/cm^2 or a higher intensity range of ~33 mW/cm^2. The resulting, relaxed state, hydrogel film was then removed from the photomask and cut into 1.5 cm diameter discs, **Figure 2-1-C**.

A Sartorius scale, as seen in **Figure 2-2**, was used to measure the weight and density of hydrogels in air and in heptane. A hanging basket apparatus was used to measure the weight of the hydrogel discs in heptane. These weights could then be used to determine the polymer volume fraction of the relaxed and swollen hydrogels, which are required for the Peppas-Merrill equation. The relaxed state weight and density were taken immediately upon cutting the 1.5 cm disc.

Figure 2-2: Sartorius Density Kit with a hanging basket apparatus used for precisely measuring weight and density.

The discs were then set to rinse for 10 days in DIH_2O on a shaker plate to remove unreacted polymers. Each day the DIH_2O was emptied and renewed with more DIH_2O.

Upon being rinsed, the hydrogel discs were set to air dry for 2 days and vacuum dried for another 7 days at 40°C and 90 kPa until reaching their dry state. Promptly after removing the dried discs from the vacuum chamber, the dried state measurements were conducted with the same approach as the relaxed state measurements. From the data collected of the hydrogel disk weights; the volume fraction in the relaxed state, $v_{2,r}$, of the discs was then determined, **Eq. 2-1**[21].

$$v_{2,r} = \frac{w_{a,d} - w_{n,d}}{w_{a,r} - w_{n,r}} \qquad \textbf{Eq. 2-1}$$

Where $w_{a,d}$ is the hydrogel weight in the dry state in air, $w_{n,d}$ is the hydrogel weight in the dry state in heptane, $w_{a,r}$ is the hydrogel weight in the relaxed state in air, and $w_{n,r}$ is the hydrogel weight in the relaxed state in heptane.

2.4 Equilibrium Swelling Studies

Equilibrium swelling studies on bulk hydrogel discs were conducted as previously reported.[35] 1X PBS was used as the solvent for the swelling studies of the PEGDMA hydrogels. Individually, each hydrogel disc was placed in a 50 ml centrifuge tube filled with 25 mL of 1X PBS and left to swell on a shaker plate for 48 hours. The hydrogels' weight and density were measured, then left to swell for a subsequent 72 hours and measured again to quantify changes. Between hour 48 and 72 no change was observed. The polymer volume fraction in the swollen state, $v_{2,s}$, **Eq. 2-2**, and the density values were recorded[21].

$$v_{2,s} = \frac{w_{a,d} - w_{h,d}}{w_{a,s} - w_{h,s}} \qquad \textbf{Eq. 2-2}$$

Where $w_{a,d}$ is the hydrogel weight in the dry state in air, $w_{h,d}$ is the hydrogel weight in the dry state in heptane, $w_{a,s}$ is the hydrogel weight in the swollen state in air, and $w_{h,s}$ is the hydrogel weight in the swollen state in heptane. The swelling ratio, *Q*, was then determined, **Eq. 2-3**.

$$Q = \frac{1}{v_{2,s}} \qquad \textbf{Eq. 2-3}$$

The Peppas-Merrill equation, **Eq. 2-4**, was then used to find the average molecular weight of the polymer chains between two adjacent crosslinks, M_c .[21]

$$\frac{1}{M_c} = \frac{2}{M_n} - \frac{\frac{v}{V_1}\left(\ln\left(1 - v_{2,s}\right) + v_{2,s} + \chi_1 v_{2,s}^2\right)}{v_{2,r}\left(\left(\frac{v_{2,s}}{v_{2,r}}\right)^{\frac{1}{3}} - \left(\frac{v_{2,s}}{2v_{2,r}}\right)\right)} \qquad \textbf{Eq. 2-4}$$

Where M_n is the number average MW of the unreacted polymer, *v* is the specific volume of the polymer, V_1 is the molar volume of the water, $v_{2,r}$ is the polymer volume fraction in the relaxed gel, $v_{2,s}$ is the polymer volume fraction in the swollen state, and χ_1, 0.426 for PEGDMA, is the free energy mixing parameter of polymer and solvent.[12] Through substitution, M_c can be used to determine the average pore size. The mathematical expression for pore size can be found by first determining $(r_0{}^2)^{1/2}$, the unperturbed end-to-end distance of the polymer chain between crosslinks, **Eq. 2-5**[21].

$$(r_0{}^2)^{1/2} = l(C_n N)^{1/2} \qquad \textbf{Eq. 2-5}$$

Where *l* is the bond length along the chain in angstroms, 1.47 Å, C_n is the Flory characteristic ratio of the polymer being used, 4 for PEGDMA, and *N* is the number of links per chain, determined by dividing M_c by the MW of the repeat units, in which case PEG is 44. And implemented in **Eq. 2-6**.

$$\xi = \alpha(r_0{}^2)^{1/2} \qquad \textbf{Eq. 2-6}$$

Where α is determined by the isotropic swelling of the hydrogel, **Eq. 2-7**.

$$\alpha = \left(v_{2,s}\right)^{-1/3} \qquad \textbf{Eq. 2-7}$$

The final pore size calculation can be determined through the combination and substitution of the previously mentioned equations, **Eq. 2-8**.

$$\xi = {v_{2,s}}^{-1/3} \left(\frac{2C_n M_c}{M_r}\right)^{1/2} l \qquad \textbf{Eq. 2-8}$$

The swelling ratio, densities, molecular weight between crosslinks, and pore size were determined for each hydrogel blend, and are presented in the results of Chapter 4.

CHAPTER 3

COMPUTATIONAL METHODS

3.1 Creation of the Computational Hydrogel Model

3.1.1 Model Overview

The motivation for creating a hydrogel model was to use it to serve as a means of understanding the increased surface area-to-volume effects of nanoscale hydrogels and to serve as a predictive model for the swelling behavior of a nanoscale hydrogel in water. Hydrogels can be complex to model due to the number of variations of polymer candidates, functionality of the crosslinks, and how polymers entangle within a network. The premise of this thesis was therefore not to model each possible candidate, rather to create a model that is able to isolate the size effects on the swelling of a hydrogel while maintaining the characteristics of a polymer network.

The structure and parameters of the hydrogel model are based on hydrogel characteristics previously described in the experimental methods section. In brief, swelling studies were performed experimentally on bulk neutral poly (ethylene glycol) di-methacrylate, PEGDMA, hydrogels, and the resulting hydrogels' density, swelling ratio, pore size, and the molecular weight between crosslinks were measured. The inherent parameters of the PEGDMA hydrogels were then implemented into the

framework of the computational model, while the outputs were used to validate the model.

Currently, hydrogel properties can be measured only at the bulk/macro scale, not at the nanoscale. To address this gap, a scalable model was developed using coarse-grained dynamics to preserve accuracy over a range of sizes while maintaining the build components for valid comparisons to be made. The objective of the model build is to swell a hydrogel from its dry state into its fully swollen, equilibrium state, in as realistic of a way as possible. The approach to building the model was to initialize a system that contained all the factors relevant to the swelling of a hydrogel – polymers, crosslinks, and water. From there, a systematic routine was followed that allowed the polymer and crosslinks to be built accurately into an energetically favorable hydrogel network. The proceeding sections are broken down into the build of the hydrogel network structure, the parameterization of the components, the engine and environment used, and the way the complete model was built to be used to test the hypothesis that nanoscale hydrogels with an increased surface area to volume ratio swell to a greater degree than their bulk counterparts. The flow chart in **Figure 3-1** summarizes the process of constructing the model. MATLAB software was used for the coding, development of the model's structure, and visualization.[69] The general-purpose particle simulation toolkit HOOMD capable of scaling to thousands of GPUs was used as the engine for the model, though only 1 GPU was used for this model.[70] VMD, visual molecular dynamics, software was used for visualizing the swelling of the hydrogel model.[71]

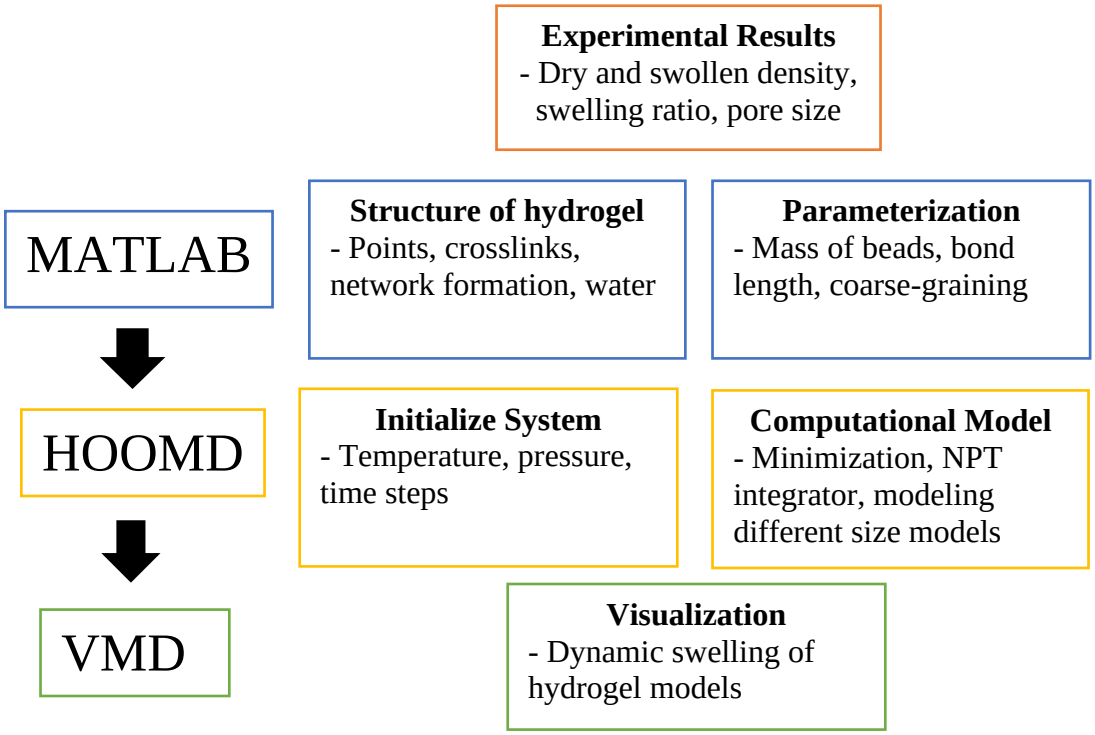

Figure 3-1: Flow chart of the computational hydrogel model progression.

3.1.2 Hydrogel Structure

The goal for the model is to represent a homogeneous hydrogel network of polymers and crosslinks that considers the random connectivity and topology of polymers. The components of the hydrogel model consist of polymer, crosslinks, and water molecules. These components are simplified into beads that will later be given an identity based on the results of molecular dynamics models of similar polymers developed by other research groups.[13,42,44,52,53,58,67,72,73] The variables to consider for constructing the build are the experimental molecular weight of the polymer, the swollen state density, the functionality of the crosslinks, and the average pore size of the given hydrogel to be modeled.

The initial step was to determine the number of nodes to place within the simulation box. The concentration of polymer/water in experimental studies affects the degree of swelling of a hydrogel[4,6,23,24,27,34,73–75]. For the model this means that the more swollen the initial structure is, the higher the final degree of swelling will be. Because of this, it is crucial that the initial hydrogel network structure be swollen to the same degree for each case to be modeled. In the case of trifunctional PEGDMA, a fully crosslinked structure will have three polymer strands for every two nodes. Each polymer strand will have 20 repeat monomers of ethylene glycol, meaning there are approximately 30 PEG units per DMA node. Therefore, an approximated number of nodes can be determined based on the molecular weight of each strand, the target density, and desired size of the simulation box. The density can be converted to beads per $Å^3$, **Eq. 3-1**.

$$\left(\frac{1.11\ g}{\mathrm{cm}^3}\right)\left(\frac{mol}{\mathrm{g}}\right)\left(\frac{6.022\times10^{23}atoms}{mol}\right)\left(\frac{\mathrm{cm}^3}{10^{24}Å^3}\right)=\frac{atoms}{Å^3} \qquad \textbf{Eq. 3-1}$$

Where the mol/g is determined by the average coarse-grained bead size of PEGDMA, and otherwise is straight forward with the number of atoms in a mol and the conversion from cm^3 to $Å^3$. Once the node density was determined, the beads were randomly spread out through the simulation box, as seen in **Figure 3-2**.

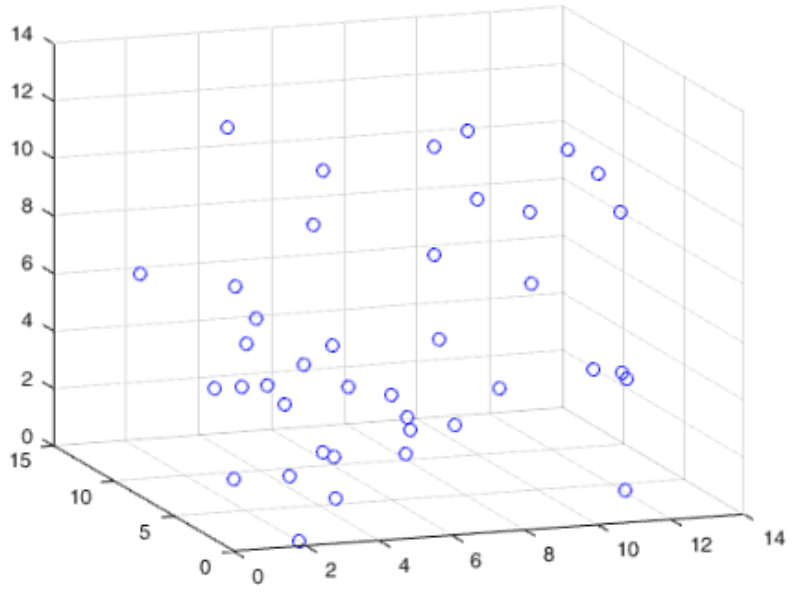

Figure 3-2: Randomly generated points in a simulation box.

The next step was to find neighbors to be crosslinked. The distance between neighbors chosen for this model ranges from 30% to 90% of the fully elongated polymer distance. The pore size derived from the average M_c by the Peppas-Merrill equation comes out to be about 30% of the elongated PEGDMA 1000 distance. The farthest neighbors at 90% polymer elongation ensured that at least 95% of the network was fully crosslinked throughout all model sizes and is reasonable since the structure will still be collapsed. Each node was then assigned 3 neighbors prioritizing the nearest distanced nodes available within the range of 30% to 90% - once a node is assigned 3 neighbors, it is no longer an option to be a chosen to be cross linked with another node. The number of neighbors was set to 3 because each polymer end can crosslink to 2 other polymer ends, as observed in the reaction in **Figure 3-5**.

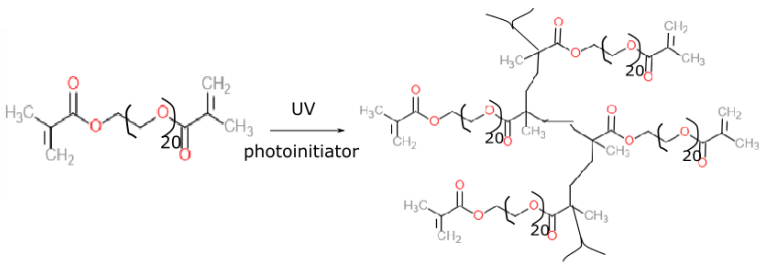

Figure 3-3: The crosslinking of PEGDMA 1000 into a branched network.

Once each node is assigned its neighbor, the polymer path between the nodes is generated. The developed code was adapted from the work of Moller Hughes that rotates a unit vector into another unit vector.[81] The code was adapted to create 3 dimensional segments of equal lengths with variable directionality to better mimic the ambiguous paths of polymer strands. The segments are alternately generated from one node towards its neighbor node and from the neighbor node towards the end of the initial segment. Each segment growth is determined by a cone-vector whose center aligns with the segment growth from the other node. The radius of the cone's base is based on the total distance between segments, the length of the segments, and the total number of segments required, as shown in **Figure 3-6**.

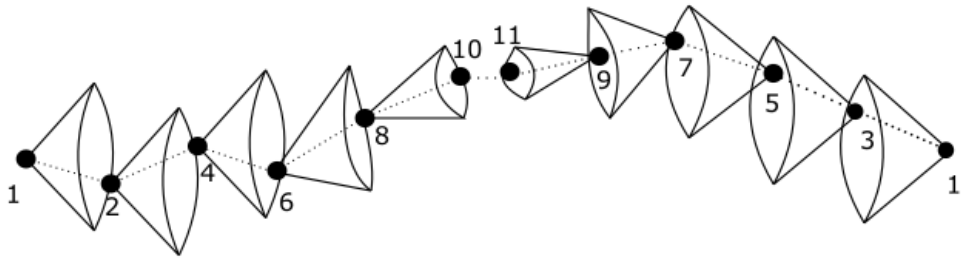

Figure 3-4: Connecting nodes alternately with equal length segments within the radius of a cone vector.

For instance, if a polymer with 10 repeat units between its crosslink points is desired, the process begins with the two neighbor nodes assigned to one another. The distance that these nodes are apart is the total displacement the 10 repeat units must cover. The initial segments generally have a wider cone radius. This radius then narrows as the total distance between nodes approaches a maximum (direct path) to be covered by the number of available segments. Once the final two points are placed, a connection is made between the two. Despite the algorithm's flexibility, the distance of paired neighbors should be large enough to prevent the segments from intertwining once they meet, but close enough that the segments do not form a direct line from node to node. The connection process is repeated for each node to its paired neighbors until a fully crosslinked network is constructed, **Figure 3-7**, which can be replicated at different sizes, **Figure 3-8**. Since the growth of segments is semi-random, it is possible for segments to leave the box parameters. For the non-periodic case, the box size is enlarged to accommodate these segments, and in the periodic case, the segments leave one box end and enter the other end through periodic boundary conditions.

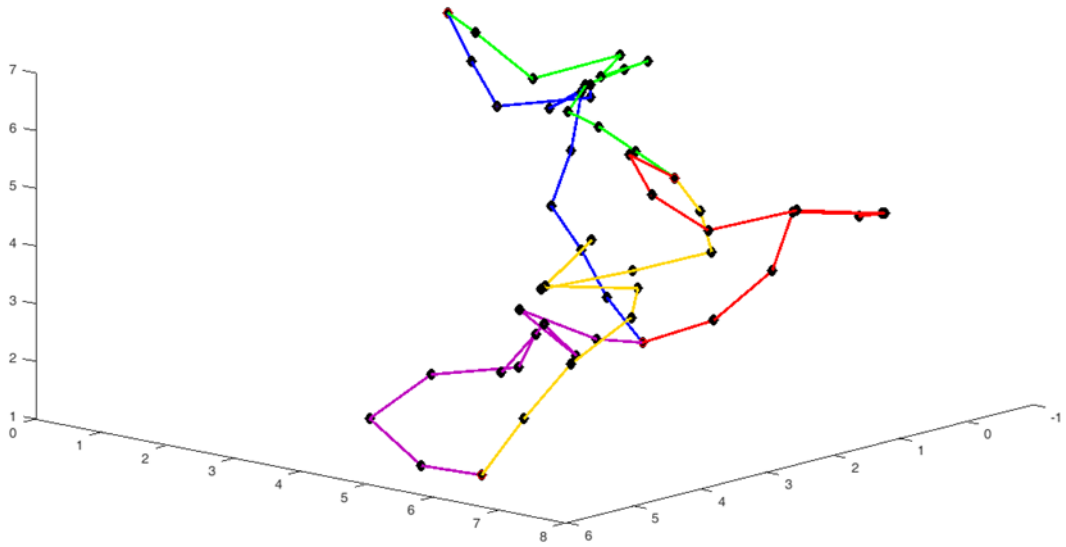

Figure 3-5: 4 Nodes with 20-monomers strands making up the polymer connection.

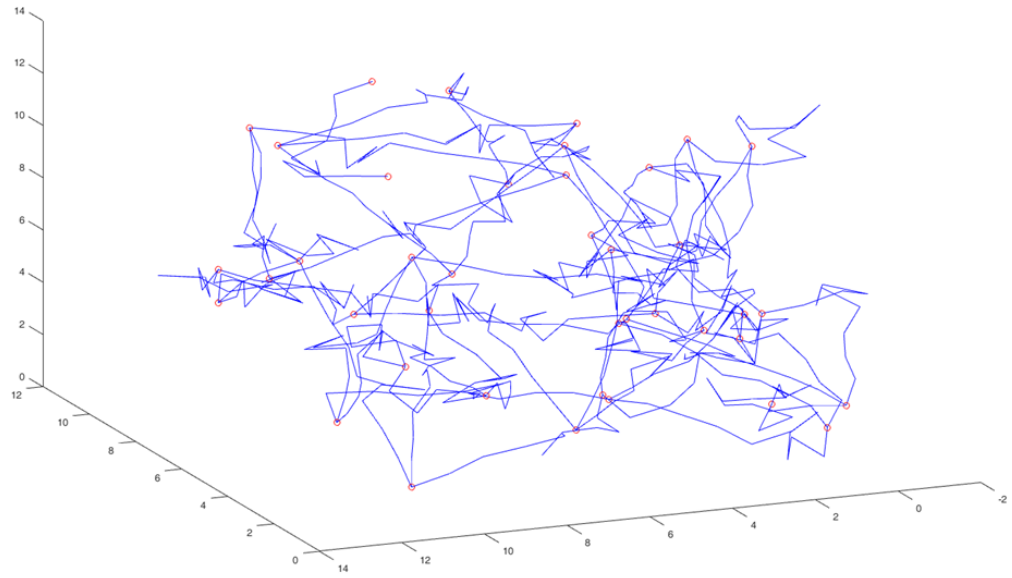

Figure 3-6: A crosslinked hydrogel containing 40 nodes and 20-monomer repeat units between nodes. Each monomer is one unit long, with each axis being in dimensionless units.

Once the fully crosslinked structure was built, water molecules were generated to either surround the hydrogel in the non-periodic case or fill the regions above and below the network in the z dimension in the periodic models. The volume of water was between 2-3 times the volume of the hydrogel structure at a density of $1.0\ g/cm^3$ converted to atoms/$Å^3$.

Two different cases were modeled, a periodic case and a non-periodic case. The periodic case models an infinite slab in two dimensions with a finite third dimension (thickness), through which water can enter the hydrogel. It does this by using periodic boundary conditions, where particles interact with an image of particles on the other side of the simulation volume (**Figure 3-7**). When an object passes through one side of the unit cell, it reappears at the opposite side with the same velocity.

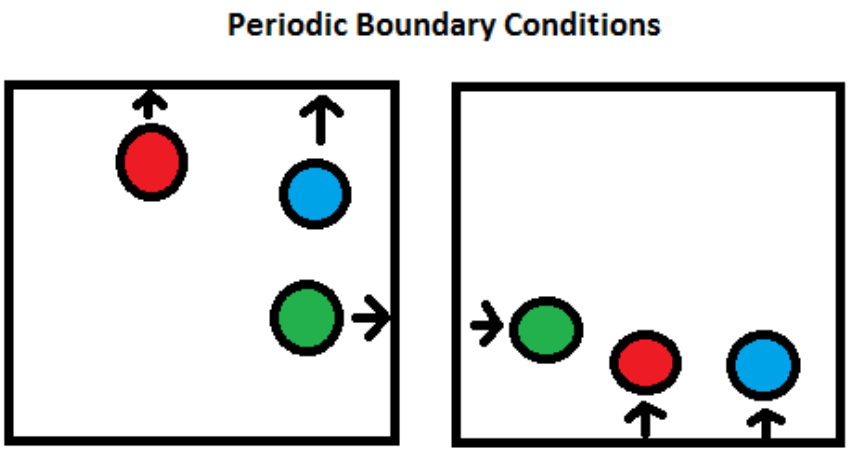

Figure 3-7: A diagram exemplifying periodic boundary conditions with particles interacting with the periodic image.

The box size for periodic boundary conditions in the case of coiled polymers must be large enough to prevent periodic interactions such that the head of the polymer is not reacting with its own tail within the length of the simulation, which could cause unphysical dynamics. The non-periodic case used a simulation volume much larger than the hydrogel so that the hydrogel never interacted with itself across that boundary, thus modeling a hydrogel which has three nanoscale dimensions versus only one for the periodic case.

3.1.3 Parameterization

Poly (ethylene glycol) di-methacrylate, PEGDMA, was chosen as the polymer for developing the experimental and computational hydrogels. Not only is it a viable polymer for drug delivery, as described in the introduction, but PEG has been extensively modeled as a polymer in solution.[6,41–45,77] The detailed background of PEG and PEG in water, was adequate in contributing to any of the elements required to parameterize this model at the coarse-grained level.[6,41–45,77] The dimethacrylate terminal, DMA, was modeled with the same interactions as PEG and appropriately modified mass and tri-functionality.

Many coarse-graining techniques exist, though the most relevant one found for this model was based on the Martini force field.[40,42,51,67,73,75,76] The Martini force field is normally based on a four-to-one mapping which means four heavy atoms are represented by a single interaction bead center[76]. PEGDMA has *n* EG units with DMA terminals. For this model, *n* is set to 20, to match experimental PEGDMA 1000. Although each PEG only has three heavy atoms, it is important to retain the functional group, and therefore a three-to-one mapping was used for the PEG repeat units. The PEG bead in this case

consists of two carbons, one oxygen and four hydrogens. The Martini force field parameter of water maps four H_2O molecules to one interaction bead center.[1–5] The mapping of the crosslinked terminals was three DMA terminals per bead with each DMA consisting of four carbons, five hydrogens, and an oxygen, though this mapping was not based on literature values.

The non-bonded interactions comprised of electrostatic forces, hydrogen bonding, and van der Waals interactions are considered through the 12-6 Lennard-Jones potential as seen in **Eq. 3-2**.[42,51,59,64,65,73,76]

$$V_{LJ} = 4\varepsilon\left[\left(\frac{\sigma}{r}\right)^{12} - \left(\frac{\sigma}{r}\right)^{6}\right] \qquad \textbf{Eq. 3-2}$$

The non-bonded interactions are considered between PEG-PEG, PEG-DMA, DMA-DMA, PEG-Water, DMA-Water, and Water-Water. Where σ is the distance where the inter-particle potential is zero (considered to be the ideal distance that two non-bonded particles can be from one another), ε is the depth of the potential well (defining the strength of the attraction or repulsion), and r is the distance between the particles[51,59,64,65]. The literature does not have coarse-graining information for DMA, so the Lennard-Jones values for PEG were also used for DMA, with only their masses differing. Since one DMA molecule has roughly 30 PEG molecules, it is expected that the values do not significantly affect the overall non-bonded interactions. The σ and ε values were based on literature values of PEG in aqueous media that were obtained by matching the distributions from all-atom simulation as seen in **Table 3-1** [40,42,43,73].

Table 3-1: Parameters for bonded and non-bonded interactions for CG PEGDMA hydrogel

	Non-bonded (LJ)		Bonded	
	σ(Å)	ε (kJ/mol)	r_0 (Å)	k (kJ/mol/Å^2)
PEG-PEG	4.15	3.375	3.3	170
PEG-DMA	4.15	3.375	3.3	170
DMA-DMA	4.15	3.375		
PEG/DMA-W_1	4.7	4		
PEG/DMA-W_2	4.7	4		
W_1-W_1	4.7	5		
W_2-W_2	5.69	5		
W_1-W_2	5.69	5		

Modeling water under the Martini force field at temperatures between 280 K and 300 K has previously led to freezing, particularly when a solid surface is present[76]. The freezing can be addressed by including anti-freeze water particles to make up about 10% of the total number of water molecules. These anti-freeze particles, labeled W2 in **Table 3-1**, are about 21% larger in size, and eliminate the freezing otherwise observed. The freezing can be identified visually, where it was observed that the water molecules form a lattice structure and do not move freely. A σ of 4.15 Å instead of the documented 4.3 Å was chosen for PEG-PEG and PEG-DMA interactions to better portray the increased density observed experimentally in the dry state of crosslinked PEGDMA hydrogels. The tested values at 4.3 Å led to densities closer to the PEGDMA polymer density (~ 1.10 g/cm^3) rather than the dry state hydrogel density of PEGDMA 1000 (~1.16 g/cm^3). All bonded interactions were considered through the harmonic bond potential as seen in **Eq. 3-3**,

$$V(r) = \frac{1}{2}\, k(r - r_0)^2 \qquad \textbf{Eq. 3-3}$$

where k is the force constant, r is the distance between to bonded particles, and r_0 is the bond rest length, as seen in **Table 3-1**.[42,43,47,56,62,63,67,75,79,80]

3.1.4 Engine

The Molecular Dynamics software used to implement the model in its coarse-grained format was HOOMD.[70,82–91] The process for running the simulation begins with a minimization to help relax the system and separate any overlapping particles that may result from the non-conventional build routine whose spatial arrangement does not represent a physical state. The minimization uses the Fast Inertial Relaxation Engine (FIRE) algorithm built into HOOMD, which minimizes a group of particles while keeping the other particles frozen, although the frozen particles will still interact with the particles being moved.[52] The minimization used takes a variably sized timestep, depending on the size of the system, and is limited to moving a particle by a maximum of 0.01 Å at each step. The minimization allows a smooth transition into the dynamics by separating overlapping particles that would otherwise hinder the simulation due to a particle being forced out of the boundary. Not all minimizations converge to a stable geometry; generally the larger systems that contained 500,000 to over 1,000,000 combined water and polymer beads posed these issues. For these, it was found that continuously changing the timestep during the minimization to larger values was an efficient method in achieving a conformation capable of continuing to the coarse-grained dynamics portion of the simulation. If the energy of the system did not change within the first few time steps of the minimization, either the timestep was modified or a new build of the hydrogel structure was made. It was found that if the energy of the system is below

5×10^8 kJ/mol, the NPT (constant number of particles, pressure, and temperature) integrator is able to continue and further relax the energy by adjusting the volume.

The NPT integrator used was the Martyna-Tobias-Klein, MTK, barostat-thermostat integrator, which allowed for a fully deformable simulation box.[41,42,44,51,52,56,64,72,73,79] The temperature was set to 293 K and the pressure was set at 1 atm for *in vitro* comparisons. The MTK, thermostat feature was given a coupling constant, τ, of 0.5 timesteps, and the barostat was given a coupling constant, τP, of 2 timesteps. The timestep for the NPT integrator of the coarse-grained dynamics was set to 10 – 50 fs based on accepted literature values.[56] The reason for having the range from 10-50 fs was to better transition from the minimization into the coarse-grained dynamics. Once the pressure and temperature of the system stabilized around the desired 1 atm and 293K, the timestep was set to 50 fs. Each simulation was run until the energy stabilized and there was no longer any swelling of the hydrogel.

3.1.5 Computational Model

The computational hydrogel models were built into 5 periodic and 5 non-periodic boundary builds. The periodic hydrogels are representative of infinitely long slabs with a variable thickness. The non-periodic hydrogels are of variable volume but are representative of their given dimensions. The hydrogels were built to be representative of the relaxed state density (polymer/volume), and were "dried" to their condensed state. The hydrogels were then labeled based on the thickness of the periodic hydrogels or the diameter of the non-periodic hydrogels. **Table 3-2** contains the dry state periodic hydrogel model builds and **Table 3-3** contains the dry state non-periodic hydrogel model builds.

Table 3-2: Dry state measurements in angstroms of the periodic model hydrogels including average distance between crosslinks, width, and thickness in angstroms.

Dry State	Distance b/w crosslinks (Å)	Width (Å)	Thickness (Å)	Polymers
Periodic 1	25.7 ± 8.8	38	107	100
Periodic 2	26.1 ± 8.7	128	168	1150
Periodic 3	26.2 ± 8.6	84	174	775
Periodic 4	25.2 ± 8.4	138	210	1750
Periodic 5	25.2 ± 8.5	86	240	2600

Table 3-3: Dry state measurements in angstroms of the non-periodic hydrogels including average distance between crosslinks and diameter in angstroms

Dry State	Distance b/w crosslinks (Å)	Diameter (Å)	Polymers
Non-periodic 1	22.8 ± 8.2	66	100
Non-periodic 2	24.9 ± 8.1	129	775
Non-periodic 3	25.3 ± 8.1	192	2600
Non-periodic 4	25.3 ± 8.4	254	6200
Non-periodic 5	26.2 ± 8.0	300	12400

The hydrogels were then swelled in water based on the previously mentioned coarse-grained parameters. The characteristics of the swollen state hydrogel models are reported in **CHAPTER 4**.

CHAPTER 4

RESULTS AND DISCUSSION

4.1 Experimental Results and Discussion

The objective of this thesis was to provide a better evaluation of micro- and nanoscale hydrogel swelling where size effects and surface area have a more pivotal role in the overall degree of swelling of hydrogels as was previously reported.[35] Data were collected from experimental swelling studies of bulk PEGDMA hydrogels to build a computational hydrogel model that could then be replicated for different hydrogel sizes. The results from the experimental swelling studies are reported and discussed, followed by an evaluation of the computational hydrogel model. The experimental results are presented with standard deviation error bars for sample sizes of 10. The bar graphs with errors bars overlapping are not statistically different according to a t-test analysis.

4.1.1 Experimental Aims

The aims of this thesis were to synthesize commonly used PEG-based hydrogels, characterize the resulting hydrogels swelling behavior, and use the data collected along with available resources to both build and validate a PEGDMA 1000 hydrogel computational model built to be representative of the experimental 25% wt. PEGDMA 1000 hydrogel. As described in **CHAPTER 2**, hydrogels with the same monomer repeat

unit, PEG, and crosslinker, DMA, were developed with a variation of factors that have an effect over the resulting hydrogel network. The variables were the percent by weight of polymer to water, the MW of PEGDMA, and the UV intensity, whose effects were then evaluated through equilibrium and dynamic swelling studies.[25,30,33,35] The effect of these factors on the resulting molecular weight between crosslinks (M_c), pore size, and swelling ratio of hydrogels have been long understood, and did not lead to any surprising results.[18,19,21,29,31,34,35,92] Based on well-established studies, assuming all other factors are constant in a neutral hydrogel, the following can be assumed:

a) If the % polymer of the hydrogel is held constant; the longer the polymer chains (attributed to larger MW in this case), the greater the pore size and M_c are, and the greater the degree of swelling is.[32,35,45]
b) If the MW of polymer used is held constant then the lower the percent by weight of polymer to water, the greater the pore size and M_c are, and the greater the degree of swelling is.[33,35,38,58]

The curing time and UV intensity required to crosslink PEGDMA are flexible based on the precursor solution compositions and hydrogel size, but crosslinking density may vary if the crosslinking reaction is not done to completion.[32,93]

Despite knowing the influence these factors have on the hydrogel matrix, the process of developing, characterizing, and analyzing the hydrogels did provide important insight on both creating and validating the computational hydrogel model. The UV intensity was tested at low intensities near 13 mW/cm^2 and at high intensities near 33 mW/cm^2 for 5 minutes with the for 2 mm thick hydrogel films. The characterized properties of the resulting hydrogels were confirmed to not be statistically different at

these intensities, with a p-value from t-tests being below 0.05, and therefore will not be presented separately in the results. Although these results were expected, this confirmation helped ensure that the crosslinking method did not add any ambiguity in the comparison of the results to follow.

4.1.2 Swelling Study Results

The swelling studies were performed to determine and compare the differences in the change in volume, the matrix structure, in the form of M_c and pore size, and the change in dry, relaxed, and swollen density of the different blends of PEGDMA hydrogels. The in air and in heptane weight measurements of the dry state, relaxed state, and swollen state hydrogels were obtained using the Sartorius density kit with an accuracy of up to 0.01 mg. These values were then used to determine the density and volume of the hydrogels and implemented into the Peppas-Merrill equation to determine the average M_c and pore size. The reported density by Sigma Aldrich for PEGDMA 750 polymer is 1.11 g/cm^3 and 1.10 g/cm^3 for PEGDMA 1000 as reported by Polysciences Inc. The hydrogels' relaxed state, dry state, and swollen state density were calculated and are summarized in **Table 4-1**.

Table 4-1: The resulting densities of 10 samplesof 25%, 30%, and 50% wt. solutions of PEGDMA with molecular weights of 750 and 1000 (± standard deviation) .

MW PEGDMA	% polymer	Relaxed density (g/cm^3)	Swollen density (g/cm^3)	Dry density (g/cm^3)
750	25	1.07 ± 0.001	1.06 ± 0.003	1.18 ± 0.008
	30	1.08 ± 0.003	1.07 ± 0.004	1.18 ± 0.003
	50	1.12 ± 0.003	1.1 ± 0.003	1.18 ± 0.004
1000	25	1.06 ± 0.003	1.05 ± 0.002	1.16 ± 0.004
	30	1.07 ± 0.001	1.06 ± 0.002	1.16 ± 0.007
	50	1.11 ± 0.001	1.08 ± 0.002	1.16 ± 0.002

The densities of the dry state hydrogels were higher than the densities of the neat PEGDMA polymers reported by Sigma Aldrich and Polysciences Inc. for both molecular weights of 750 and 1000 with t-test p-values < 0.05. The density of the hydrogels in the dry state was attributed to the molecular weight of the polymer, regardless of the percentage weight of polymer to water of the initial hydrogel solution, **Figure 4-1**.

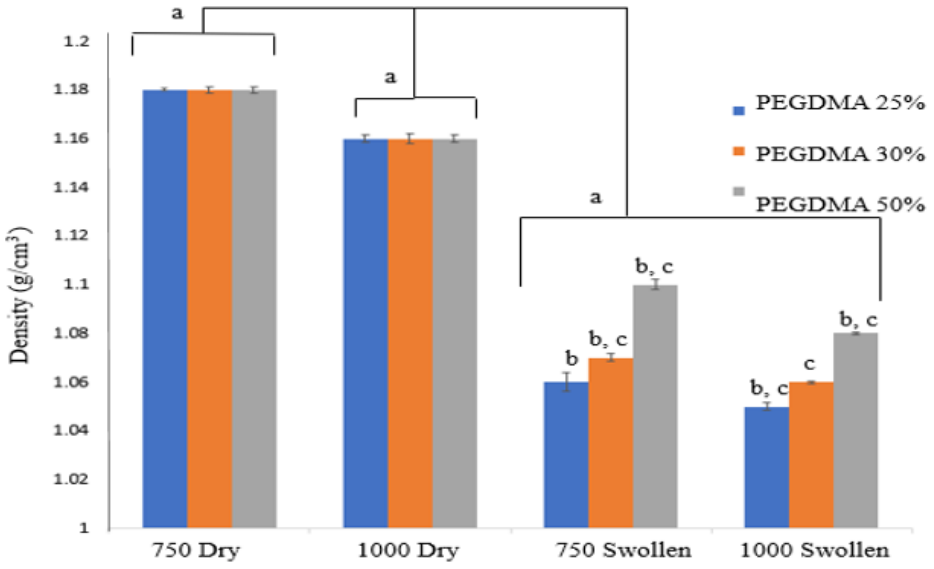

Figure 4-1: Density of the dry and swollen state of PEGDMA 750 and PEGDMA 1000 hydrogels at 25%, 30%, and 50% polymer weight to volume. The matching letters 'a','b, and 'c' signify statistical difference from student t-test with p-values below 0.05, where n=10.

Unlike the dry state densities, the swollen state densities differed based on the molecular weight and percent by weight of polymer by weight. In the swollen state, density tends to increase, with both 750 and 1000 molecular weight hydrogels, as the percent polymer increases. This increase is expected since the denser precursor solution would lead to a denser hydrogel.

The calculated molecular weight between crosslinks, M_c, and the pore size, ξ, followed the expected trend, with statistical significance, that the larger the MW and the lower the percent polymer, the greater the M_c and pore size (**Figure 4-2** and **Figure 4-3**).

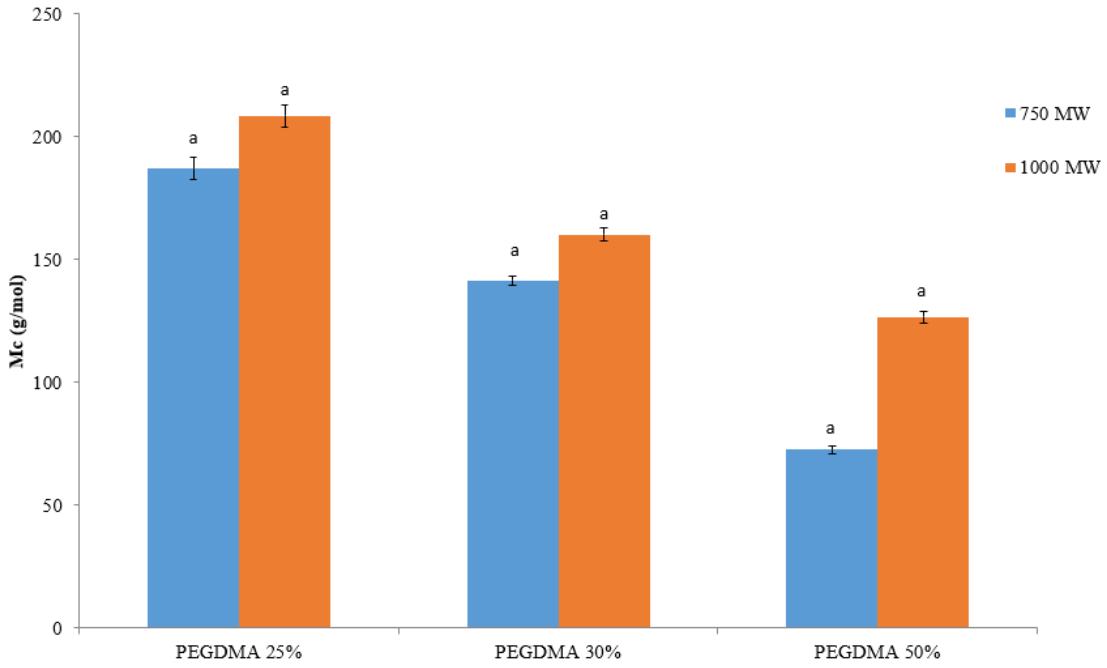

Figure 4-2: Average molecular weight between crosslinks of PEGDMA 750 hydrogels and PEGDMA 1000 hydrogels of 25%, 30%, and 50% weight of polymer to volume composition. The matching letter 'a' signifies statistical difference from student t-test with p-values below 0.05, where n=10.

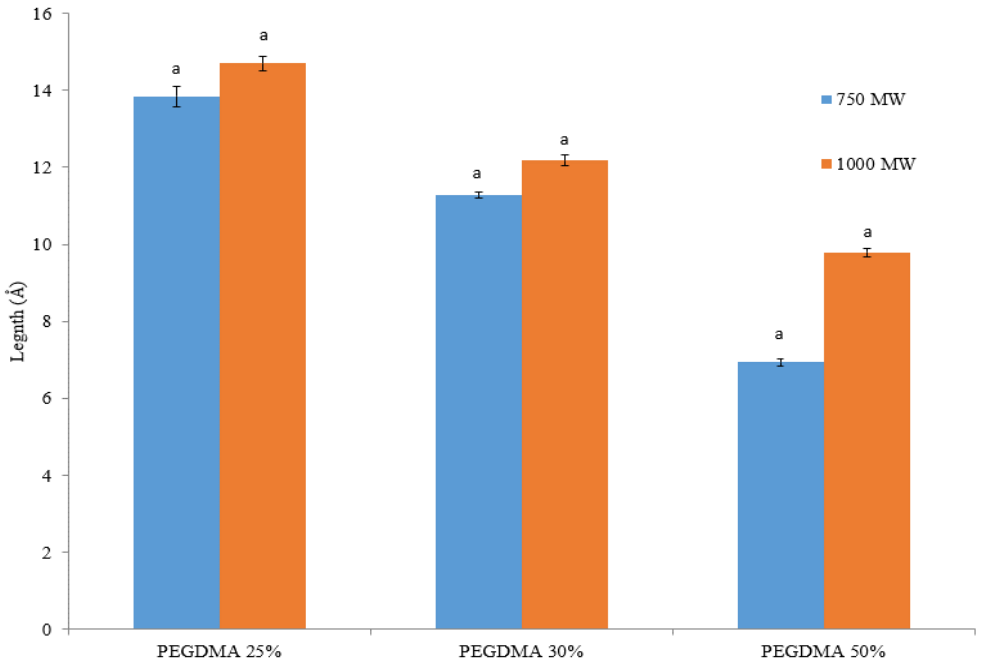

Figure 4-3: The average pore size of different blends of PEGDMA hydrogels with respect to molecular weight and percent by weight of polymer to water. The matching letter a signifies statistical difference from student t-test with p-values below 0.05, where n=10.

The volumetric swelling ratio of a hydrogel measures the degree of change from the dry state to the swollen state. The 25% PEGDMA blends of 750 and 1000 MW led to p-value above 0.05. For all other cases, tests were statistically significant ($p > 0.05$) that for each respective percent polymer larger PEGDMA strand molecular weight corresponds to larger swelling ratio, and lower PEGDMA hydrogel percent polymer for each respective molecular weight corresponds to larger the swelling ratio (**Figure 4-5**).

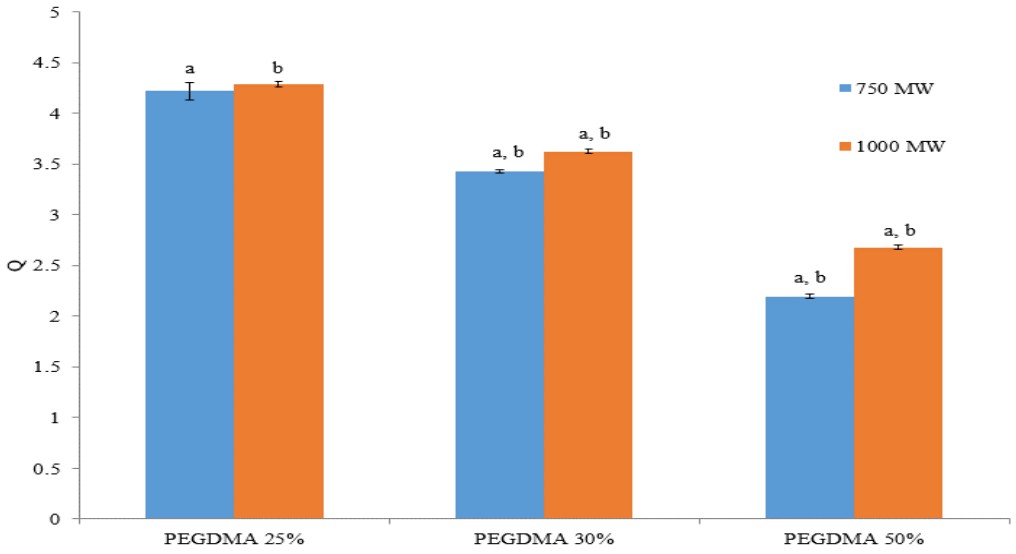

Figure 4-4: The volumetric swelling ratio of swollen to dry PEGDMA hydrogel blends. Match letters 'a and b' signify statistical difference from student t-test with p-values > 0.05, where n=10.

The rate of swelling for each hydrogel blend was tested through dynamic swelling studies, which were done in neutral PBS buffer solution over 100 minutes since PEGDMA hydrogels are not ionic hydrogels. The rate of change is sharpest as the dry PEGDMA hydrogels are initially placed in the solution and remain relatively stagnant after the one-hour mark, as seen in **Figure 4-5**.

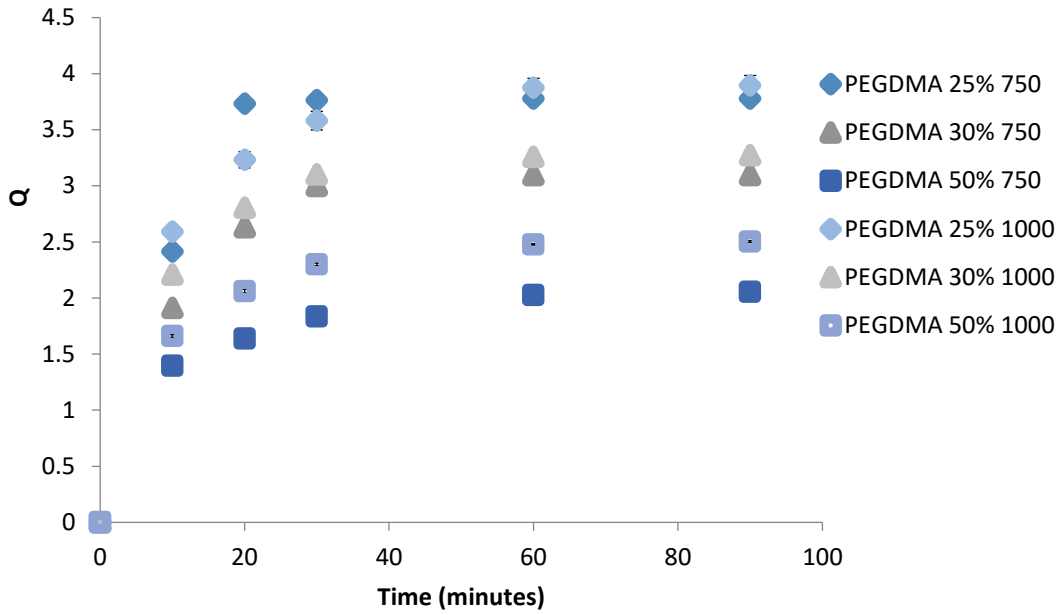

Figure 4-5: Dynamic swelling of different blends of PEGDMA hydrogels from their dry state to their equilibrium state in pH 7.4 PBS average values from n= 10 are plotted with stand deviation error bars with p-values < 0.05.

The dynamic swelling studies proceeded as expected and matched the trends of the equilibrium swelling studies and the expected trends from previous reports.[25,35,40,41] The graph reveals how most of the swelling occurs in the first 20 minutes of the dry hydrogel being in solvent.

Overall, the experimental work contributed to the computational hydrogel model in two ways, the design and the validation of the model. The design of the computational hydrogel model was intended to isolate the effects of size and surface area on swelling, meaning all other contributing factors would need to be isolated. For this thesis, a computational hydrogel model representative of the 25% wt. PEGDMA 1000 hydrogels was developed. The validity of the computational hydrogel model could be tested with

the experimental dry state density and the swelling ratio of the 25% wt. PEGDMA 1000 hydrogels.

4.2 Computational Results and Discussion

4.2.1 Computational Design

The computational models were built in MATLAB, simulated in HOOMD, visualized in VMD, and analyzed with MATLAB. The goal of the computational models was to examine the differences in swelling observed in variably sized hydrogels in the nanometer range. Two types of hydrogel models were created as described in Chapter 2, periodic hydrogels, representative of infinite slabs with variable thickness, and non-periodic hydrogels of specified dimensions. As stated in the creation of the model, each hydrogel was built in an expanded, "relaxed state" cube shape without water within the hydrogel structure, **Figure 4-6**.

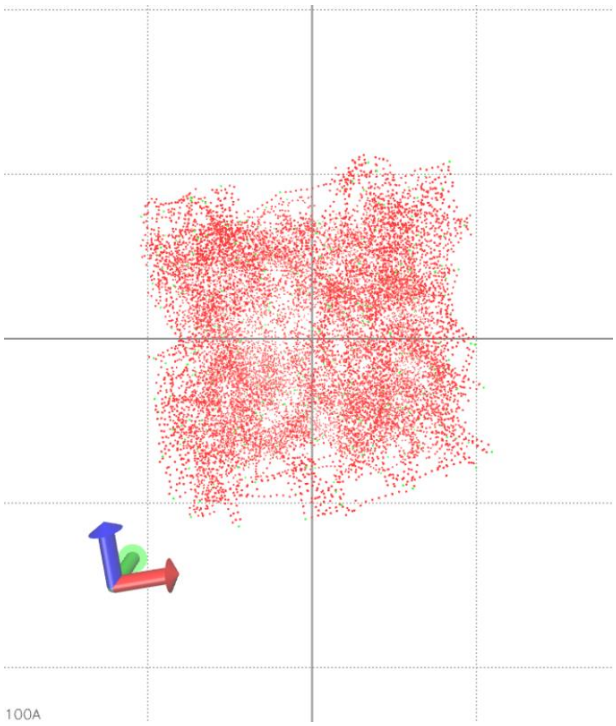

Figure 4-6: Expanded state of hydrogel before compressing it into the dry state.

From the relaxed state, the hydrogel models were compressed into the dry state, as done experimentally, by making the water-polymer interactions repulsive and only allowing the attraction between water-water and polymer-polymer. Although each initial build of the hydrogel was expanded to fit a cube, the hydrogels with the periodic build conditions compressed into slabs in their dry state. On the other hand, the non-periodic hydrogels compressed into spheres from their cube-expanded form. The compressed dry state was then used as the starting point of the swelling simulation. Water particles entered the periodic hydrogel builds from the ±z axes, **Figure 4-7**.

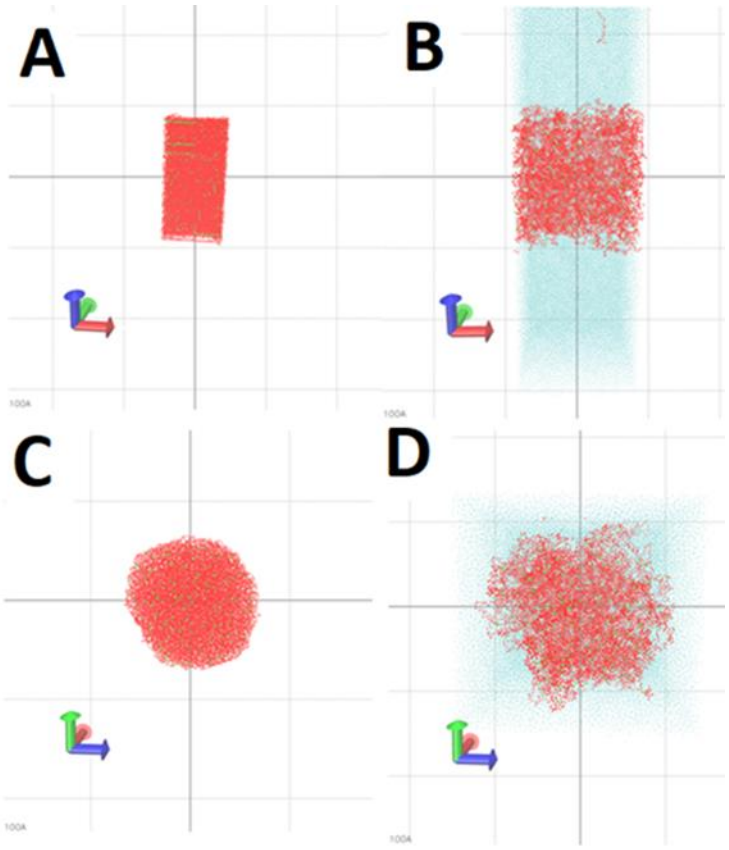

Figure 4-7: Dry (A) and swollen (B) state of a periodic hydrogel with water coming in from only the z dimensions. Dry (C) and swollen (D) state of a non-periodic hydrogel with water coming in from all interfaces. Red is poly(ethylene glycol), green is di-methacrylate crosslinks, and cyan is water.

Within both types of hydrogels, non-periodic and periodic, a subset of sizes and thicknesses were made to examine the effects of size and surface area on hydrogel swelling. Ten total hydrogel builds were created, five periodic hydrogel builds and five

non-periodic hydrogel builds. **Table 4-3** presents the periodic hydrogels arranged by increasing thickness.

Table 4-2: Dry state measurements in angstroms of the periodic hydrogels including number of polymers, average distance between crosslinks, volume, width, and height.

Dry State	Distance b/w crosslinks (Å)	Width (Å)	Thickness (Å)	Polymers
Periodic 1	25.7 ± 8.8	38	107	100
Periodic 2	26.1 ± 8.7	128	168	1150
Periodic 3	26.2 ± 8.6	84	174	775
Periodic 4	25.2 ± 8.4	138	210	1750
Periodic 5	25.2 ± 8.5	86	240	2600

Table 4-4 presents the dry state values of the non-periodic hydrogels, arranged by increasing volume.

Table 4-3: Dry state measurements in angstroms of the non-periodic hydrogels including average distance between crosslinks, width, and height in angstroms.

Dry State	Distance b/w crosslinks (Å)	Diameter (Å)	Polymers
Non-periodic 1	22.8 ± 8.2	66	100
Non-periodic 2	24.9 ± 8.1	129	775
Non-periodic 3	25.3 ± 8.1	192	2600
Non-periodic 4	25.3 ± 8.4	254	6200
Non-periodic 5	26.2 ± 8.0	300	12400

The 2-dimensional size comparisons of the non-periodic hydrogels and periodic hydrogels can be observed in **Figure 4-9** and **Figure 4-10**.

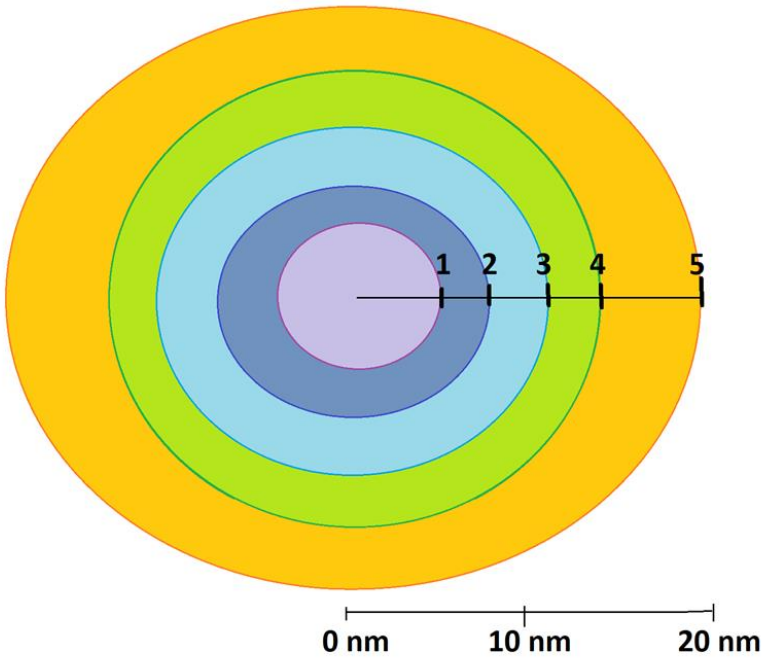

Figure 4-8: Size comparisons by radii lengths of the 5 non-periodic hydrogel builds.

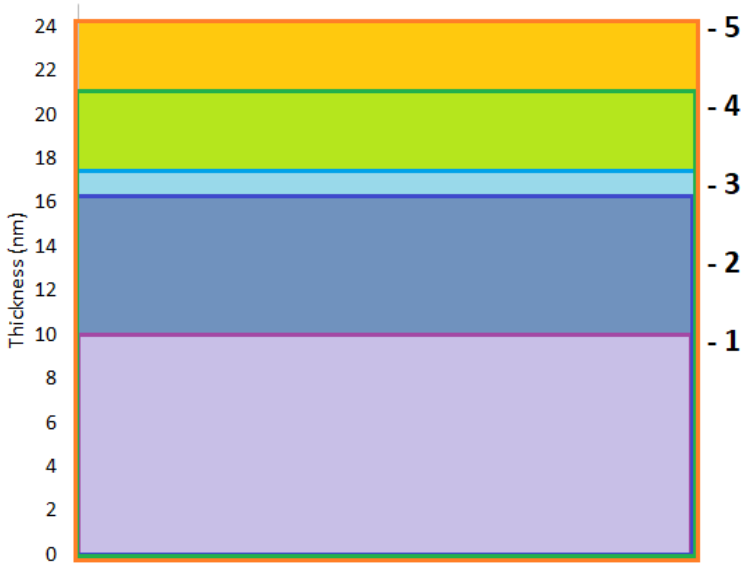

Figure 4-9: Size comparisons by thickness (nm) of the 5 periodic hydrogel infinite slabs.

The parameters used for representing the coarse grained hydrogel models in HOOMD were based on values for poly(ethylene glycol) in water, however, these parameters had not been used to study the size effects on hydrogel swelling.[15,40,42–44,51,52,55–57,59,61,63,67,72,73,75,76,76] In order to confirm the model was representative of a PEGDMA 1000 hydrogel, the density of the dry state were measured and compared against experimental values. For the non-periodic case, the hydrogel model was divided into spherical shells whose surface were 10 Å apart (e.g. center-10, 10-20, 20-30, 30-surface). The volume of each shell was calculated and the number of polymer beads within each shell was used to determine the density of the shell. For the periodic case, the hydrogel model was divided into layers (xy slices) from the center layer, to determine density based on the distance from the center layer. Slices were made from the center to the top and from the center to the bottom. The volume and density of polymer were summed for the mirrored layers (e.g. 0 to 10 was summed with -10 to 0, 10 to 20 with -20 to -10) to measure a true density based on distance from the center. The density gradient from the center to the surface of the non-periodic and periodic hydrogels were calculated in MATLAB and can be seen in **Figure 4-10** and **Figure 4-11**.

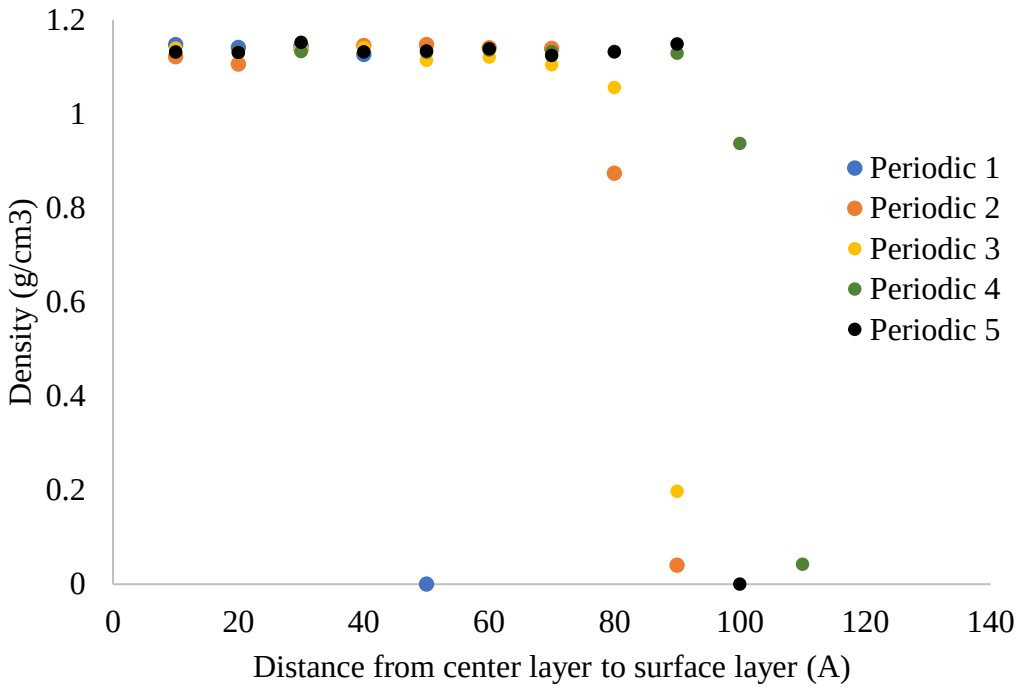

Figure 4-10: The dry state density of periodic hydrogel models from the center layer to the outside layer. Also effectively portraying half the thickness of the periodic hydrogel sample.

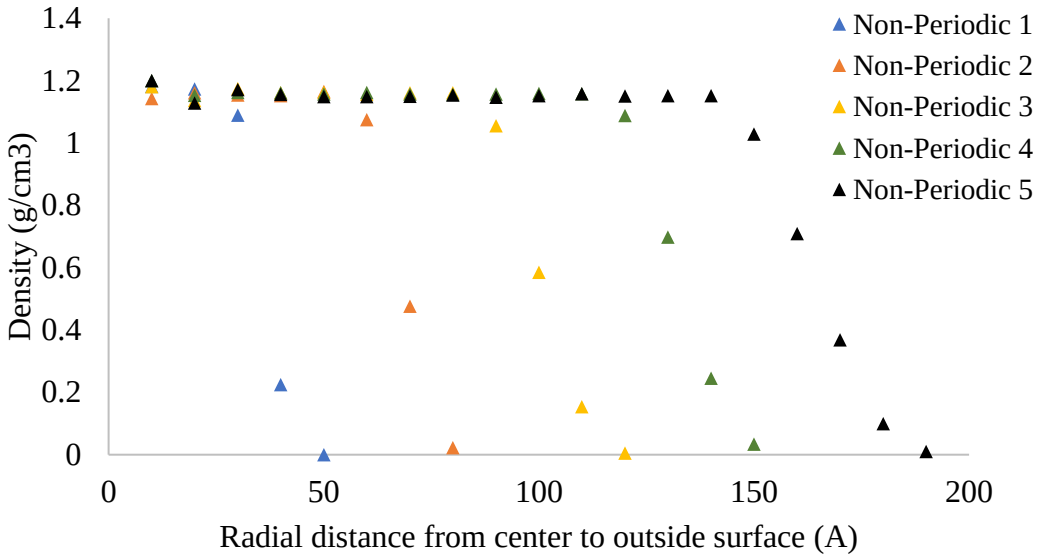

Figure 4-11: The dry state density of non-periodic hydrogel models from the center to the outside layer. Also portraying the radii of the given "spherical" non-periodic hydrogel models.

The core density, defined as the region with stagnant density, of the dry state of both periodic and non-periodic hydrogels fluctuated between 1.14 g/cm^3 and 1.17 g/cm^3 for all the samples measured between 10 Å and 40 Å from the center, which is near the desired 1.16 g/cm^3 for all the periodic and non-periodic samples. For the non-periodic hydrogel models, the distance from the center was taken radially, and for the periodic hydrogel models, the distances were taken from the center to the top and bottom layers since the x and y dimensions were not surfaces. The values obtained were in the range of the calculated experimental density of the PEGDMA 1000 hydrogels, and all sizes equilibrated at about the same target density, which was observed experimentally as well for all the PEGDMA 1000 hydrogel blends. The fluctuation in density per shell is expected since each shell is either 10 Å thick for non-periodic models or 20 Å thick for periodic models. Time was not directly measured for these studies. Instead, each model was run to completion, which was determined by no change in the density gradient. However, for future use of the model, more timesteps were required for larger simulations containing more polymer strands and water molecules. For reference, the largest hydrogel model contained over 12,000 polymers and took over 150 million, with 5 fs time steps to fully swell and equilibrate.

The overall swelling ratio was measured for each sample through a direct volume calculation and through an indirect approach by dividing the core dry state density by the core swollen state density. The volume calculations are more precise for the dry state hydrogel models since the swollen state hydrogel models contain dangling polymer strands at the surface that skew the volume calculation. The distance between crosslinks,

volume, density, width, and height were then measured and averaged for the swollen state hydrogels, **Table 4-4**.

Table 4-4: Swollen state periodic and non-periodic hydrogel measurements containing the distance between crosslinks, core density, width, and height.

Swollen	Distance b/w crosslinks (Å)	Density (g/cm^3)	Width (Å)	Height (Å)
Periodic 1	31.87 ± 7.9	0.31	80	112
Periodic 2	32.3 ± 7.9	0.3	232	212
Periodic 3	32.5 ± 8.0	0.28	158	203
Periodic 4	31.8 ± 8.1	0.32	232	276
Periodic 5	32.7 ± 8.0	0.25	158	286
Non-Periodic 1	29.6 ± 7.5	0.2641	104	112
Non-Periodic 2	31.6 ± 8.1	0.2664	200	235
Non-Periodic 3	31.9 ± 7.9	0.2865	302	300
Non-Periodic 4	32.5 ± 7.8	0.2912	414	403
Non-Periodic 5	31.8 ± 7.9	0.299	538	520

The ratio change of the swollen state to the dry state was then calculated (**Table 4-5**).

Table 4-5: The swollen state to dry state ratio change measurements of the periodic and non-periodic computational hydrogel models. The change in width, height, distance between crosslinks, volume (Q), and volume based on change in core density were calculated.

	Change in width	Change in height	Change in distance b/w crosslinks	Q	Density based Q
Periodic 1	2.11	1.05	1.24	3.92	3.69
Periodic 2	1.81	1.26	1.24	3.98	3.79
Periodic 3	1.88	1.17	1.24	4.42	4.07
Periodic 4	1.68	1.31	1.26	3.25	3.54
Periodic 5	1.84	1.19	1.30	4.81	4.61
Non-Periodic 1	1.58	1.67	1.30	5.55	4.44
Non-Periodic 2	1.55	1.87	1.27	4.68	4.33
Non-Periodic 3	1.57	1.57	1.26	4.14	4.10
Non-Periodic 4	1.68	1.15	1.28	4.55	3.99
Non-Periodic 5	2.41	1.40	1.27	4.17	3.92

The periodic hydrogels, and for the two largest non-periodic hydrogels swell to a greater extent in the width than in height. The anisotropic swelling can be mostly attributed to artifacts of the build routine that create the hydrogel in a cube shape, meaning the final shape of the swollen hydrogel would swell to the same shape. Otherwise, it would be expected thermodynamically that the final state be spherical.

The effects of size on swelling were further investigated by plotting the density gradient of polymer of the swollen hydrogel models, **Figure 4-12**.

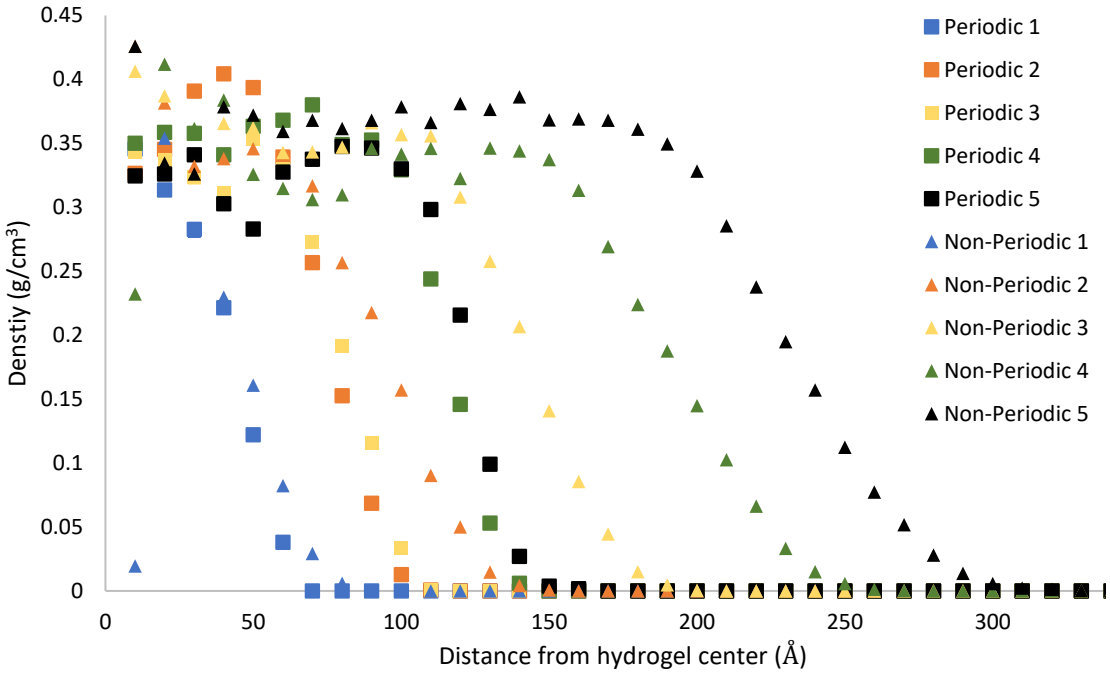

Figure 4-12: The swollen state density gradient of periodic and non-periodic hydrogel models from the center to the outside.

Each hydrogel model has a core density between 0.32 g/cm^3 and 0.43 g/cm^3, and a diminishing density towards the edges of the hydrogel models. The periodic hydrogels with only two interfaces with water have a gradient surface of ~5 nm as opposed to a ~7 nm gradient for the non-periodic hydrogels. The core volume change can be measured by

dividing the core density of the dry state by the core density of the swollen state. Although the swollen state core density of polymer for all the hydrogel model sizes and types is nearly the same, further investigation into the edges led to promising size effect conclusions. The density can be described by two distinct regions: 1) the core, where density is roughly constant and equal for all cases, and 2) the surface, where density decreases from the core density to zero. For bulk samples, the surface comprises a very small fraction of the overall volume, but for nanoscale samples the surface region makes up a significant portion of the volume. These effects were then quantified based on the measured gradient length. For the quantification, the non-periodic hydrogels are considered as spheres and the periodic hydrogels are considered as cuboids, since the dry states of these builds are spheres and cuboids respectively. The gradient density of the hydrogels is considered from where the surface density is 0.10 g/cm^3 to the point at which the core density is 0.35 g/cm^3. The range was estimated to be around 40-60 angstroms from the surface of the non-periodic hydrogels' radii of the non-periodic hydrogels' radii (**Figure 4-13**).

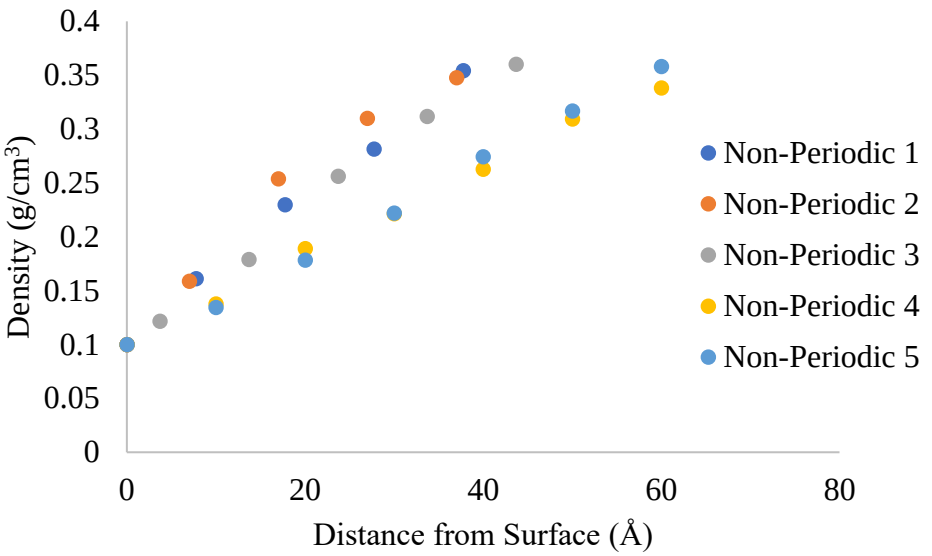

Figure 4-13: The surface density gradient of the 5 non-periodic hydrogel builds.

The range from the surface of the periodic hydrogel was between 40-50 angstroms, **Figure 4-14**.

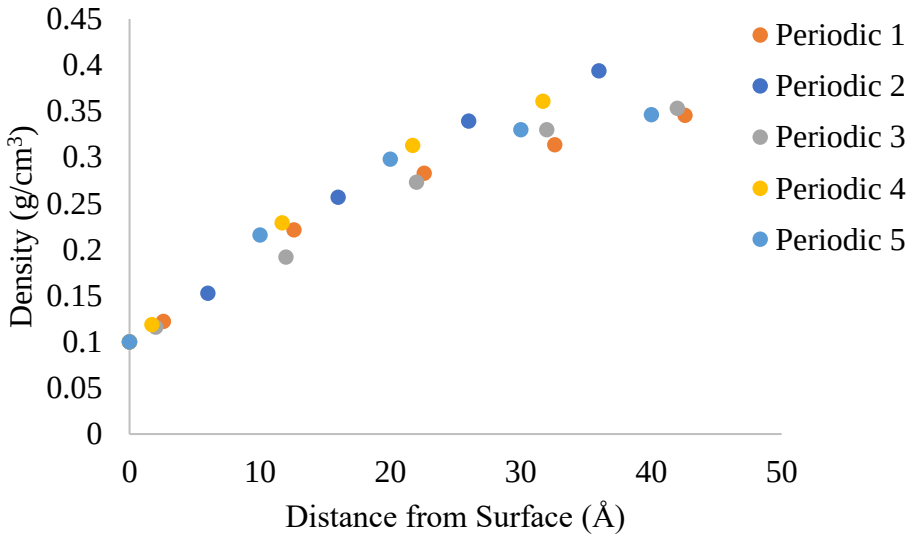

Figure 4-14: The surface density gradient of the 5 periodic hydrogel builds.

The surface effects for the non-periodic hydrogels is accounted for across the

entire surface, and only two surfaces for the periodic hydrogels. Although these surface volumes increase with an increase in overall size of the hydrogel, the surface area to volume ratio decreases.

After a series of calculations, the surface volume can be related to the overall swelling ratio of the nanoscale hydrogels to make a predictive curve based on the non-periodic and periodic computational model results. The overall swelling ratio, *Q*, was determined by taking the weighted average of the bulk swelling ratio and the surface layer swelling ratio. *Q* can be determined by taking the ratio of the dry state density to the swollen state density, **Eq. 4-1**.

$$Q = \frac{\text{dry state density}}{\text{swollen state density}} \qquad \textbf{Eq. 4-1}$$

A surface *Q* was determined by substituting the dry state density of 1.16 g/cm^3 and the average swollen density of the surface layer, using the average of the density values from **Figure 4-13** and **Figure 4-14** respectively. The bulk *Q* was determined by substituting the dry state density of 1.16 g/cm^3 and the bulk swollen density of 0.35 g/cm^3. The total volume for the periodic hydrogels was considered for a cuboid with a known length, width, and height, and total volume for the non-periodic hydrogels was considered for a sphere with a known radius. The surface layer volume (V_{SL}) for the non-periodic hydrogels was estimated based on the 5-7 nm surface layer, **Eq. 4-2**.

$$\text{Non} - \text{periodic}\, V_{SL} = \left(\frac{4}{3}\pi r^3\right) - \left(\frac{4}{3}\pi(r - l_{\text{Surface}})^3\right) \qquad \textbf{Eq. 4-2}$$

Where *r* is the radius of the non-periodic hydrogel and $l_{Surface}$ is the length of the surface layer. The surface layer volume (V_{SL}) of the periodic hydrogels was estimated based on the 5 nm surface layer, **Eq. 4-3**.

$$\text{Periodic}\, V_{SL} = 2\, l\, w\, h_{\text{Surface}} \qquad \textbf{Eq. 4-3}$$

Where *l* is the length, *w* is the width, and h_{Surface} is the surface height. Once the surface volumes were determined, **Eq. 4-4** was used to estimate Q_{Total} for the model hydrogels,

$$Q_{\text{Total}} = \left(\text{Q}_{\text{Surface}} \times \frac{V_{SL}}{V_{Total}}\right) + \left(Q_{\text{Bulk}} \times \left(1 - \frac{V_{SL}}{V_{\text{Total}}}\right)\right) \qquad \textbf{Eq. 4-4}$$

Where V_{SL} is the surface layer volume and V_{Total} is the total volume of the hydrogel.

A curve was then made to fit both the periodic and non-periodic hydrogel models to capture how size affects the overall swelling ratio of hydrogels, based on the previous calculations.

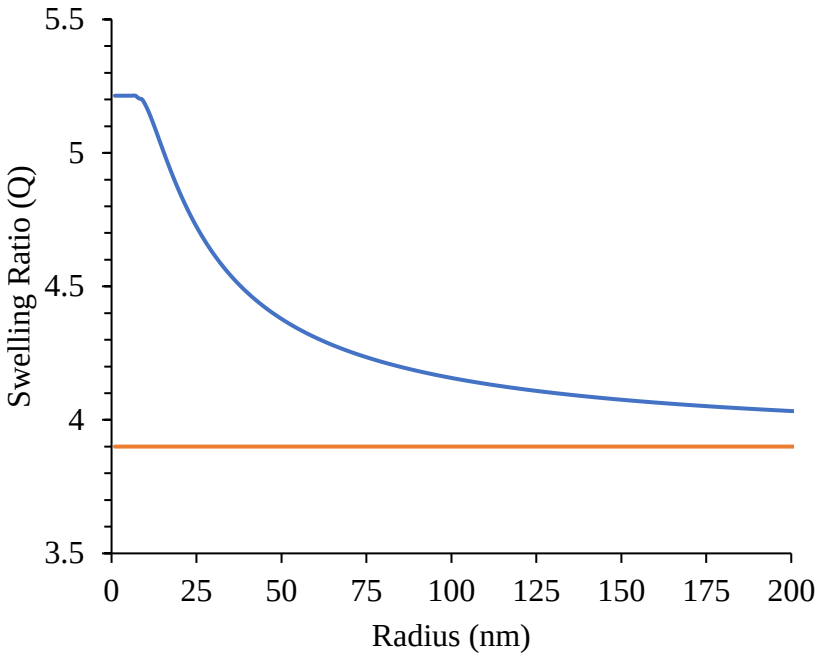

Figure 4-15: The predicted swelling ratio of nanoscale hydrogels based on the weighted density gradient of the non-periodic computational hydrogel models. The gradient distance is averaged to be around 5-7 nm from the surface. The blue line represents the predicted swelling ratio of 25% PEGDMA 1000 nanoscale hydrogels of given radii. The orange line represents the average swelling ratio of the "bulk" experimental 25% PEGDMA 1000 hydrogels.

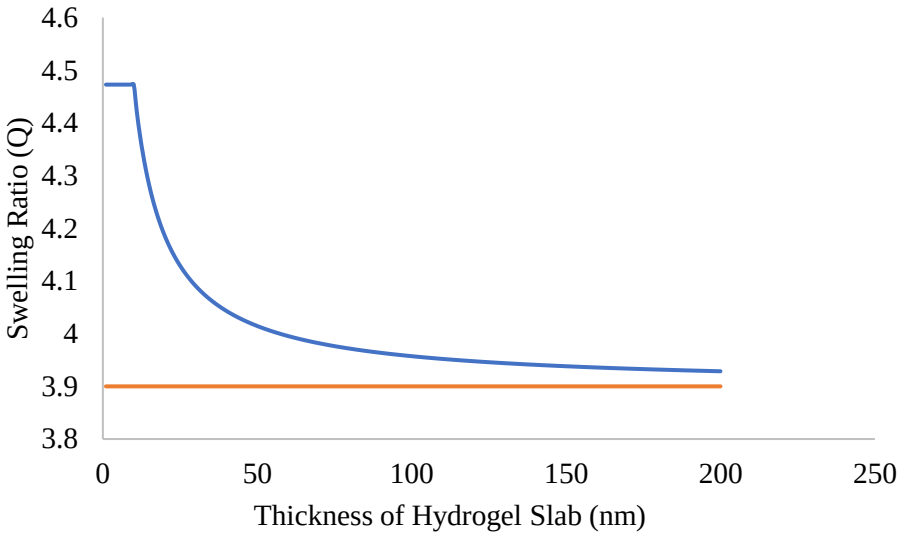

Figure 4-16: The predicted swelling ratio of nanoscale hydrogel slabs based on the weighted density gradient of the periodic computational hydrogel models. The gradient range is averaged around 5 nm from the surface. The blue line represents the predicted swelling ratio of 25% PEGDMA 1000 hydrogel slabs of given thicknesses. The orange line represents the average swelling ratio of the "bulk" experimental 25% PEGDMA 1000 hydrogels.

As observed in **Figure 4-15** and **Figure 4-16**, the density gradient at the surface of nanoscale hydrogels will influence the overall swelling ratio. The flat line at the beginning of both curves is representative of the volumes in which the surface layer volume constitutes the total volume. These surface effects can account for up to a 30-40% increase in overall swelling ratio for hydrogels with a thickness between 0-10 nm and are still dominant into the length scale of 100 nm (50 nm radius), contributing to a 10% increase in swelling.

Two main deductions can be made on the surface effects observed. 1) The swelling at the surface of hydrogels is larger than at the core. This implies that the pore size at the surface will be greater than the pore size at the core. 2) The swelling at the surface largely affects the overall swelling of nanoscale hydrogels. The more surfaces in contact with solvent and the smaller the nanoscale hydrogel, the greater the overall

swelling ratio of the hydrogel. These deductions can then be translated to their effects on drug delivery. Deduction 1 relates to the size of the drug for loading and release and the rate of drug release, which need to be evaluated differently in the nanoscale based on the model. Deduction 2 relates to the overall size of the hydrogel. In drug delivery, there is a size range between 80-200 nm that should be considered for optimizing drug distribution, toxicity, and targeting ability.

The hydrogel model was analyzed against itself, experimental bulk hydrogel swelling studies, and nanoscale hydrogel swelling studies by Caldorera-Moore *et al*. Before considering the analysis, the limitations and differences between the model and experimental work must be addressed. In the model, the hydrogel was able to crosslink at a 95% or greater success rate, the distribution of crosslinks and polymer paths are generated computationally, and the initial polymer concentration may not reflect the same experimental density. Most crucial to the comparison of experimental and computational hydrogel swelling is in the fact that the percent polymer to water of the precursor hydrogel solution will strongly affect the swelling capability of the hydrogel. Despite knowing the concentration of polymer in the precursor solution, once the precursor solution is cured into a hydrogel, potentially unreacted polymer, or a surplus or deficit of water, would change the initial concentration of the hydrogel. The initial concentration affects the swelling capability of the hydrogel, which leaves ambiguity in replicating the process computationally. The hydrogel models in this work were also only modeling PEGDMA 1000 to be representative of the 25%-30% hydrogel blends, meaning that an increase or decrease in either the molecular weight or % by weight of polymer to water may affect the swelling curve, however, the same trend would be expected, possibly at a

higher or lower magnitude.

The experimental values of the bulk PEGDMA hydrogels were useful in confirming the validity of the model. The experimental dry state density of all PEGDMA 1000 hydrogels was around 1.16 g/cm^3 regardless of the % by weight of polymer to water. The density was achieved in the computational models through the "drying" phase of the molecular dynamics meaning the coarse-grained parameters correctly portrayed the PEGDMA polymers. The accuracy of the model was also investigated by comparing the swelling ratios of the experimental 25% wt. and 30% wt. PEGDMA 1000 hydrogels to the computational swelling. Based on the average change in volume (excluding the surfaces), the computational model swelled between the range of the 25% wt. and 30% wt. PEGDMA 1000 hydrogels' swelling ratios (Q) of (3.6 – 4.3). Although the computational model was to be more representative of the 25% wt. PEGDMA 1000 hydrogel swelling, the increased degree of crosslinking in the computational model probably causes the discrepancy since increased crosslinking would increase the elastic constraints and therefore the hydrogel would swell less.

The results from the model, coincide well with the observations by Caldorera-Moore *et al*. that hydrogels with all dimensions in the 100 nm size range swell significantly more than their bulk counterparts.[35] For this study, 33% by volume poly(ethylene glycol) diacrylate, PEGDA, hydrogels were fabricated at relaxed state sizes of 100x100x100 nm, 400x100x100 nm, and 800x100x100 nm (length, width, height) and imaged with AFM and scanning electron microscopy (SEM) with wet cells. The length swelling was roughly 20% larger for the hydrogel with an initial length of 100 nm in comparison to the bulk (~1.4/1.14). The 100x100x100 nm hydrogel would be most comparable to the non- periodic hydrogel curve at a radius of 50 nm, though the model at

a radius of 50 nm would have a smaller surface area to volume ratio. When considering the differences of the experimental setup of the hydrogels fabricated by Caldorera-Moore *et al.* and the computational hydrogel model, the overall trends of increased swelling in the smaller dimensions correlate well.

The hypothesis that nanoscale hydrogels with an increased surface area to volume ratio swell to a greater extent than their bulk counterparts was confirmed with the computational hydrogel model. The relation was made between the degree of swelling experienced by the surface layer and the ratio of the surface layer to the total volume of the hydrogel. The extent of the overall swelling ratio difference between nanoscale hydrogels and their bulk counterparts is determined by the length scale of the hydrogel surfaces in contact with the solvent.

CHAPTER 5

CONCLUSIONS AND FUTURE WORK

5.1 Discussion

The objective of this thesis was to investigate the effects of size and surface area to volume ratio on the swelling of nanoscale hydrogels in comparison to their bulk counterparts. One of the most widely used characterization methods of hydrogels is swelling studies, which can be used in conjunction with the Peppas-Merrill equation to determine the hydrogel structure. The Peppas-Merrill equation uses theory of mixing and elasticity to predict the average molecular weight between crosslinks and pore size of neutral hydrogels. The motivation for creating this computational hydrogel model was to investigate the effects of increased surface area to volume ratio in nanoscale hydrogels as well as the validity of using the Peppas-Merrill equation to characterize nanoscale hydrogels. The approach for this thesis was to 1) synthesize PEGDMA hydrogels, 2) conduct swelling studies with the PEGDMA hydrogels, 3) use experimental data and coarse-grained parameters to develop a hydrogel model, 4) validate the hydrogel model, 5) analyze the effects of size and surface area to volume ratio on swelling.

In this work, the dominating surface effects of nanoscale hydrogels were investigated by creating a computational hydrogel model capable of simulating the swelling of hydrogel networks in water between the length scales of 5-50 nm. For the experimental portion, swelling studies were conducted on PEGDMA 750 and 1000 MW

hydrogels, which were characterized by their density, molecular weight between crosslinks, pore size, and swelling ratio. A coarse-grained computational PEGDMA hydrogel model representative of the 25%-30% wt. of polymer to water of PEGDMA 1000 hydrogels that could be scaled to different sizes were then developed. Periodic (1 dimension in the nanoscale) and non-periodic (3 dimensions in the nanoscale) hydrogel builds were made between 5 and 50 nm to investigate both size and surface area to volume ratio effect on swelling. By keeping all factors (MW, build routine, initial density, coarse grained parameters) the same and only scaling size, we isolated the size effects. The accuracy of the model was confirmed by comparing the experimental swelling ratios, Q, of the 25% and 30% PEGDMA 1000 hydrogels to the computational models' core swelling ratio, which fell between the two. The dry state density of the experimental 25% PEGDMA 1000 matched well with the computational model, which also helped to confirm the accuracy of the coarse-grained parameters of the bonded and non-bonded polymers.

The computational hydrogel model was then used to investigate how size affects the swelling ratio. It was observed that the surface layer volume of hydrogels does not have the same density as the core volume of the hydrogel, rather, a density gradient roughly 4-7 nm thick exists near the surface. For bulk hydrogels, the surface effects can be neglected since the gradient persists for less than ~7 nm from the surface. However, for nanoscale hydrogels (0 - 200 nm diameter), this surface layer can allow for up to roughly 40% increased swelling. The comparison between the periodic and non-periodic hydrogel builds was used to measure the significance of the surface area to volume ratio. At equilibrium, the surface layer in contact with water is what contributes most to the

increased swelling in nanoscale hydrogels. The more surface exposed to water, the greater the total swelling of the nanoscale hydrogels. The swollen core density remains relatively constant among all the hydrogel builds at equilibrium.

5.2 Conclusion

Ultimately, the computational hydrogel model was successful in representing a 25%-30% PEGDMA 1000 hydrogel. The model confirmed the hypothesis that nanoscale hydrogels swell to a greater extent than their bulk counterparts. The gradient density observed at the surface is what causes the increased swelling observed in nanoscale hydrogels. As the size decreases into the nanoscale, the surface area to volume ratio increases, and the more prominent the surface area to volume ratio, the greater the overall swelling of the hydrogel. The implications of the surface differences may also be of importance for bulk hydrogel studies and uses. Based on the findings of this model, the Peppas-Merrill equation, though useful for determining bulk characteristics, it is not an effective way of determining the average pore size of nanoscale hydrogels. Being that pore size is related to density, it is expected that the average pore size on the surface layer volume is different than the average pore size of the core volume. With the increase in surface pore size, the rate of diffusion out of the nanoscale hydrogel network and the size of drug therapeutics being loaded into the nanoscale hydrogel network must be considered differently than for their bulk counterparts.

5.3 Future Work

The objective of this thesis was to provide an alternative method for characterizing nanoscale hydrogels, to better understand the role of size on the swelling of hydrogels. Despite the intended use for this computational model, the computational

model itself is not limited to being used to study size effects on swelling. The model itself can be broken down into the build components and the representation of the components. With minor modifications on the build side, the polymer network can consist of different molecular weight polymers, node functionality, % polymer, and sizes. On the coarse-graining side, the type of polymer and network contents can be modified to address other areas of interest in hydrogel modeling, even to the extent of modeling a drug and simulating its release from the hydrogel network for predictive use of drug diffusion.

As presented in the results, the model can be analyzed to determine the average distance between chemical crosslinks. The Peppas-Merrill equation currently uses swelling study information and theory to determine an estimated M_c and pore size for a given hydrogel sample. With the design of a better analysis tool that considers physical entanglements, these features could be known for the hydrogel model based on the molecular dynamics rather than thermodynamic and elastic theory.

The hydrogel computational model as a whole was able to accomplish the goal of this thesis. In the process of creating an extensive hydrogel model that isolates the effects size has on hydrogel swelling, a model capable of investigating the effects of using higher or lower molecular weight polymers, lesser or greater functionality of the crosslinker, percent crosslinking, % polymer to volume, and size on swelling was created. With the numerous variations of hydrogels based on polymer type, molecular weight, concentration, functionality, size, etc., it is possible to construct these hydrogels computationally and predict how the swelling will occur. The hydrogel networks could be created and analyzed without the cost, equipment, or experimentalists' time, with desirably a high degree of accuracy.

BIBLIOGRAPHY

1. Magnani M. Drug delivery and targeting system. *Emerg Ther Targets*. 1998;2(1):145-146. doi:10.1517/14728222.2.1.145.

2. Brannon-peppas L. Polymers in Controlled Drug Delivery. 1997;(November).

3. Wadhwa H. Global Markets and Technologies for Advanced Drug Delivery Systems.

4. Langer R, Peppas NA. Advances in Biomaterials, Drug Delivery, and Bionanotechnology. *AIChE J*. 2003;49(12):2990-3006. doi:10.1002/aic.690491202.

5. Koetting MC, Peters JT, Steichen SD, Peppas NA. Stimulus-responsive hydrogels: Theory, modern advances, and applications. *Mater Sci Eng R Rep*. 2015;93:1-49. doi:10.1016/j.mser.2015.04.001.

6. Knop K, Hoogenboom R, Fischer D, Schubert US. Poly(ethylene glycol) in drug delivery: Pros and cons as well as potential alternatives. *Angew Chemie - Int Ed*. 2010;49(36):6288-6308. doi:10.1002/anie.200902672.

7. Shi J, Votruba AR, Farokhzad OC, Langer R. Nanotechnology in drug delivery and tissue engineering: from discovery to applications. *Nano Lett*. 2010;10(9):3223-3230. doi:10.1021/nl102184c.

8. Gaharwar AK, Peppas NA, Khademhosseini A. Nanocomposite hydrogels for biomedical applications. *Biotechnol Bioeng*. 2014;111(3):441-453. doi:10.1002/bit.25160.

9. Oh JK, Lee DI, Park JM. Biopolymer-based microgels/nanogels for drug delivery applications. *Prog Polym Sci*. 2009;34(12):1261-1282. doi:10.1016/j.progpolymsci.2009.08.001.

10. Brannon-Peppas L, Peppas NA. Equilibrium swelling behavior of pH-sensitive hydrogels. *Chem Eng Sci*. 1991;46(3):715-722. doi:10.1016/0009-2509(91)80177-Z.

11. Oh JK, Drumright R, Siegwart DJ, Matyjaszewski K. The development of microgels/nanogels for drug delivery applications. *Prog Polym Sci*. 2008;33(4):448-477. doi:10.1016/j.progpolymsci.2008.01.002.

12. Peppas NA, Hilt JZ, Khademhosseini A, Langer R. Hydrogels in biology and medicine: From molecular principles to bionanotechnology. *Adv Mater*. 2006;18(11):1345-1360. doi:10.1002/adma.200501612.

13. Yeh PD, Alexeev A. Mesoscale modelling of environmentally responsive hydrogels: emerging applications. *Chem Commun*. 2015;51(50):10083-10095. doi:10.1039/C5CC01027F.

14. Zhao X. Multi-scale multi-mechanism design of tough hydrogels: building dissipation into stretchy networks. *Soft Matter*. 2014;10(5):672-687. doi:10.1039/C3SM52272E.

15. Walter J, Ermatchkov V, Vrabec J, Hasse H. Molecular Dynamics and Experimental Study of Conformation Change of Poly (N-isopropylacrylamide) -hydrogels in Water.

16. Saul JM, Williams DF. Hydrogels in Regenerative Medicine. In: *Handbook of Polymer Applications in Medicine and Medical Devices*. ; 2013. doi:10.1016/B978-0-323-22805-3.00012-8.

17. Hoffman AS. Hydrogels for biomedical applications . *Adv Drug Deliv Rev*. 2012;64:18-23. doi:10.1016/j.addr.2012.09.010.

18. Hoare TR, Kohane DS. Hydrogels in drug delivery: Progress and challenges. *Polym with aligned carbon Nanotub Act Compos Mater*. 2008;49:1993-2007. doi:10.1016/j.polymer.2008.01.027.

19. Siepmann J, Peppas NA. Higuchi equation : Derivation , applications , use and misuse. *Int J Pharm*. 2011;418(1):6-12. doi:10.1016/j.ijpharm.2011.03.051.

20. Buwalda SJ, Boere KWM, Dijkstra PJ, Feijen J, Vermonden T, Hennink WE. Hydrogels in a historical perspective: From simple networks to smart materials. *J Control Release*. 2014;190(November 2015):254-273. doi:10.1016/j.jconrel.2014.03.052.

21. Peppas NA. Hydrogel. *An Introd to Mater Med*. 2012:35-42.

22. Bäckström S, Benavente J, Berg RW, et al. Tailoring Properties of Biocompatible PEG-DMA Hydrogels with UV Light. *Mater Sci Appl*. 2012;3(June):425-431. doi:10.4236/msa.2012.36060.

23. Peppas NA, Bures P, Leobandung W, Ichikawa H. Hydrogels in pharmaceutical formulations. *Eur J Pharm Biopharm*. 2000;50(1):27-46. http://www.ncbi.nlm.nih.gov/pubmed/10840191. Accessed January 30, 2019.

24. Caldorera-moore M, Peppas NA. Micro- and nanotechnologies for intelligent and responsive biomaterial-based medical systems. *Adv Drug Deliv Rev*. 2009;61(15):1391-1401. doi:10.1016/j.addr.2009.09.002.

25. Khare AR, Peppas NA. Swelling/deswelling of anionic copolymer gels. *Biomaterials*. 1995;16(7):559-567. doi:10.1016/0142-9612(95)91130-Q.

26. *Polymers in Controlled Drug Delivery*.; 1997. http://www.ing.unitn.it/~luttero/materialifunzionali/DrugRelease.pdf. Accessed January 30, 2019.

27. Koetting MC, Peters JT, Steichen SD, Peppas NA. Stimulus-responsive hydrogels : Theory , modern advances , and applications. 2019:1-49. doi:10.1016/j.mser.2015.04.001.

28. Hoffman AS. The origins and evolution of "controlled" drug delivery systems. *J Control Release*. 2008;132(3):153-163. doi:10.1016/j.jconrel.2008.08.012.

29. Ganji F, Vasheghani-Farahani S, Vasheghani-Farahani E. Theoretical Description of Hydrogel Swelling: A Review. *Iran Polym J*. 2010;19(5):375-398. doi:10.1007/s12303-009-0004-6.

30. De SK, Aluru NR, Johnson B, Crone WC, Beebe DJ, Moore J. Equilibrium Swelling and Kinetics of pH-Responsive Hydrogels : Models , Experiments , and Simulations. 2002;11(5):544-555.

31. Ward MA, Georgiou TK. Thermoresponsive polymers for biomedical applications. *Polymers (Basel)*. 2011;3(3):1215-1242. doi:10.3390/polym3031215.

32. Anseth KS, Kline LM, Walker T a., Anderson KJ, Bowman CN. Reaction Kinetics and Volume Relaxation during Polymerizations of Multiethylene Glycol Dimethacrylates. *Macromolecules*. 1995;28(7):2491-2499. doi:10.1021/ma00111a050.

33. Heimbuck AM, Priddy-arrington TR, Benjamin J, Caldorera-moore ME. PT CR. *Mater Sci Eng C*. 2018;(2019):#pagerange#. doi:10.1016/j.msec.2018.12.119.

34. Carr DA, Peppas NA. Molecular Structure of Physiologically-Responsive Hydrogels Controls Diffusive Behavior. 2019;9(5):497-505. doi:10.1002/mabi.200800235.

35. Caldorera-Moore M, Kang MK, Moore Z, et al. Swelling behavior of nanoscale, shape- and size-specific, hydrogel particles fabricated using imprint lithography. *Soft Matter*. 2011;7(6):2879-2887. doi:10.1039/c0sm01185a.

36. Baysal K, Aroguz AZ, Adiguzel Z, Baysal BM. Chitosan/alginate crosslinked hydrogels: Preparation, characterization and application for cell growth purposes. *Int J Biol Macromol*. 2013;59. doi:10.1016/j.ijbiomac.2013.04.073.

37. Duynhoven JPM Van. The impact of freeze-drying on microstructure and rehydration properties of carrot. *FRIN*. 2012;49(2):687-693. doi:10.1016/j.foodres.2012.08.019.

38. Peppas NA, Merrill EW. Crosslinked poly(vinyl alcohol) hydrogels as swollen elastic networks. *J Appl Polym Sci*. 1977;21(7):1763-1770. doi:10.1002/app.1977.070210704.

39. Berger J, Reist M, Mayer JM, Felt O, Peppas NA, Gurny R. Structure and interactions in covalently and ionically crosslinked chitosan hydrogels for biomedical applications. doi:10.1016/S0939-6411(03)00161-9.

40. Prasitnok K, Wilson MR. A coarse-grained model for polyethylene glycol in bulk water and at a water/air interface. *Phys Chem Chem Phys*. 2013;15(40):17093-17104. doi:10.1039/c3cp52958d.

41. Ou X, Han Q, Dai H-H, Wang J. Molecular dynamic simulations of the water absorbency of hydrogels. *J Mol Model*. 2015;21(9):231. doi:10.1007/s00894-015-2784-0.

42. Rossi G, Fuchs PFJ, Barnoud J, Monticelli L. A coarse-grained MARTINI model of polyethylene glycol and of polyoxyethylene alkyl ether surfactants. *J Phys Chem B*. 2012;116(49):14353-14362. doi:10.1021/jp3095165.

43. Choi E, Mondal J, Yethiraj A. Coarse-grained models for aqueous polyethylene glycol solutions. *J Phys Chem B*. 2014;118(1):323-329. doi:10.1021/jp408392b.

44. Wang Q, Keffer DJ, Nicholson DM. A coarse-grained model for polyethylene glycol polymer. *J Chem Phys*. 2011;135(21). doi:10.1063/1.3664623.

45. Lee H, Venable RM, MacKerell AD, Pastor RW. Molecular dynamics studies of polyethylene oxide and polyethylene glycol: Hydrodynamic radius and shape anisotropy. *Biophys J*. 2008;95(4):1590-1599. doi:10.1529/biophysj.108.133025.

46. Mark JE, Erman B. *Oxford Handbooks Online Elastomers and Rubberlike Elasticity*.; 2017. doi:10.1093/oxfordhb/9780199667925.013.8.

47. Westermann S, Richter D. On the Length Scale Dependence of Microscopic Strain by SANS. 2001:2186-2194.

48. Ramzi A, Hakiki A, Bastide J, Boue F, Le L. Uniaxial Extension of End-Linked Polystyrene Networks Containing Deuterated Free Chains Studied by Small-Angle Neutron Scattering : Effect of the Network Chains and the Size of the Free Chains. 1997;9297(96):2963-2977.

49. Darinskii AA, Zarembo A, Balabaev NK. Molecular Dynamic Simulation of Side-Chain Liquid Crystalline Elastomer Under Load. 2007:101-109. doi:10.1002/masy.200750610.

50. Leibler L. Scattering by Deformed Swollen Gels : Butterfly Isointensity Patterns. 1990:1821-1825.

51. Chiu S, Scott HL, Jakobsson E. A Coarse-Grained Model Based on Morse Potential for Water and n -Alkanes. *J Chem Theory Comput*. 2010;6:851-863. doi:10.1021/ct900475p.

52. Glotzer S, Paul W. Molecular and Mesoscale Simulation Methods for Polymer Materials. *Annu Rev Mater Res*. 2002;32:401-436. doi:10.1146/annurev.matsci.32.010802.112213.

53. Computational Modelling: Technological Futures.

54. Akkermans RLC. Mesoscale model parameters from molecular cluster calculations. *J Chem Phys*. 2008;128(24):244904. doi:10.1063/1.2943211.

55. Nielsen SO, Lopez CF, Srinivas G, Klein ML. Coarse grain models and the computer simulation of soft materials. *J Phys Condens Matter*. 2004;16(15). doi:10.1088/0953-8984/16/15/R03.

56. Winger M, Trzesniak D, Baron R, Van Gunsteren WF. On using a too large integration time step in molecular dynamics simulations of coarse-grained molecular models. *Phys Chem Chem Phys*. 2009;11(12):1-8. doi:10.1039/b818713d.

57. McCabe C, Hadley KR. On the investigation of coarse-grained models for water: Balancing computational efficiency and the retention of structural properties. *J Phys Chem B*. 2010;114(13):4590-4599. doi:10.1021/jp911894a.

58. Shinoda W, Devane R, Klein ML. Multi-property fitting and parameterization of a coarse grained model for aqueous surfactants. *Mol Simul*. 2007;33(1-2):27-36. doi:10.1080/08927020601054050.

59. Luo C, Sommer JU. Coding coarse grained polymer model for LAMMPS and its application to polymer crystallization. *Comput Phys Commun*. 2009;180(8):1382-1391. doi:10.1016/j.cpc.2009.01.028.

60. Doi H, Okuwaki K, Naito T, Saitou S. A portable code for dissipative particle dynamics (DPD) simulations with additional specific interactions. :1-33.

61. Reith D, Meyer H, Mu F. Mapping Atomistic to Coarse-Grained Polymer Models Using Automatic Simplex Optimization To Fit Structural Properties. 2001:2335-2345.

62. Reith D, Mathias P, Florian M. Deriving effective mesoscale potentials from atomistic simulations. 2014;(November 1996).

63. Mu F, Reith D, Pu M. from Atomistic Simulations. 2003.

64. Papadopoulou A, Becker ED, Lupkowski M, Van Swol F. Molecular dynamics and Monte Carlo simulations in the grand canonical ensemble: Local versus global control. *J Chem Phys*. 1993;98(6):4897-4908. doi:10.1063/1.464945.

65. Lee JW, Nilson RH, Templeton JA, Griffiths SK, Kung A, Wong BM. Comparison of molecular dynamics with classical density functional and Poisson-Boltzmann theories of the electric double layer in nanochannels. *J Chem Theory Comput*. 2012;8(6):2012-2022. doi:10.1021/ct3001156.

66. Liyana-Arachchi TP, Jamadagni SN, Eike D, Koenig PH, Ilja Siepmann J. Liquid-liquid equilibria for soft-repulsive particles: Improved equation of state and methodology for representing molecules of different sizes and chemistry in dissipative particle dynamics. *J Chem Phys*. 2015;142(4). doi:10.1063/1.4905918.

67. Kmiecik S, Gront D, Kolinski M, et al. Coarse-Grained Protein Models and Their Applications. 2016. doi:10.1021/acs.chemrev.6b00163.

68. Caccavo D, Cascone S, Lamberti G, Barba AA. Modeling the drug release from hydrogel-based matrices. *Mol Pharm*. 2015;12(2). doi:10.1021/mp500563n.

69. The Language of Technical Computing : Computation, Visualization, Programming : Installation Guide for UNIX Version 5. 1996.

70. Anderson JA, Lorenz CD, Travesset A. General purpose molecular dynamics simulations fully implemented on graphics processing units. *J Comput Phys*. 2008;227(10):5342-5359. doi:10.1016/j.jcp.2008.01.047.

71. HUMP96.pdf.

72. Pérez-Aparicio R, Colmenero J, Alvarez F, Padding JT, Briels WJ. Chain dynamics of poly(ethylene-alt-propylene) melts by means of coarse-grained simulations based on atomistic molecular dynamics. *J Chem Phys*. 2010;132(2). doi:10.1063/1.3280067.

73. Lee H, Vries AH De, Marrink S, Pastor RW. A coarse-grained model for polyethylene oxide : conformation and hydrodynamics. *Blood*. 2009:13186-13194.

74. Lazutin AA, Glagolev MK, Vasilevskaya V V, Khokhlov AR. Hypercrosslinked polystyrene networks : An atomistic molecular dynamics simulation combined with a mapping / reverse mapping procedure Hypercrosslinked polystyrene networks : An atomistic molecular dynamics simulation combined with a mapping / reverse mapping procedure. 2014;134903:0-8. doi:10.1063/1.4869695.

75. Hadley KR, McCabe C. Coarse-Grained Molecular Models of Water: A Review. *Mol Simul*. 2012;38(8-9):671-681. doi:10.1080/08927022.2012.671942.

76. Marrink SJ, Risselada HJ, Yefimov S, Tieleman DP, De Vries AH. The MARTINI force field: Coarse grained model for biomolecular simulations. *J Phys Chem B*. 2007;111(27):7812-7824. doi:10.1021/jp071097f.

77. Lee H, Venable RM, Mackerell AD, Pastor RW, Pastor RW. Molecular dynamics studies of polyethylene oxide and polyethylene glycol: hydrodynamic radius and shape anisotropy. *Biophys J*. 2008;95(4):1590-1599. doi:10.1529/biophysj.108.133025.

78. Español P, Warren PB. Perspective: Dissipative particle dynamics. *J Chem Phys*. 2017;146(15). doi:10.1063/1.4979514.

79. Ren P, Ponder JW. Polarizable Atomic Multipole Water Model for Molecular Mechanics Simulation. 2003:5933-5947.

80. Choe JI, Kim B. Determination of proper time step for molecular dynamics simulation. *Bull Korean Chem Soc*. 2000;21(4):419-424.

81. Hughes M. Efficiently Building a Matrix to Rotate One Vector to Another. http://www.acm.org/jgt/papers/MollerHughes99. Published 1999.

82. Howard MP, Panagiotopoulos AZ, Nikoubashman A. Efficient mesoscale hydrodynamics: Multiparticle collision dynamics with massively parallel GPU acceleration. *Comput Phys Commun*. 2018;230:10-20. doi:10.1016/j.cpc.2018.04.009.

83. Spellings M, Marson RL, Anderson JA, Glotzer SC. GPU accelerated Discrete Element Method (DEM) molecular dynamics for conservative, faceted particle simulations. *J Comput Phys*. 2017;334:460-467. doi:10.1016/j.jcp.2017.01.014.

84. LeBard DN, Levine BG, Mertmann P, et al. Self-assembly of coarse-grained ionic surfactants accelerated by graphics processing units. *Soft Matter*. 2012;8(8):2385-2397. doi:10.1039/C1SM06787G.

85. Phillips CL, Anderson JA, Glotzer SC. Pseudo-random number generation for Brownian Dynamics and Dissipative Particle Dynamics simulations on GPU devices. *J Comput Phys*. 2011;230(19):7191-7201. doi:10.1016/j.jcp.2011.05.021.

86. Levine BG, LeBard DN, DeVane R, Shinoda W, Kohlmeyer A, Klein ML. Micellization Studied by GPU-Accelerated Coarse-Grained Molecular Dynamics. *J Chem Theory Comput*. 2011;7(12):4135-4145. doi:10.1021/ct2005193.

87. Morozov IV, Kazennov AM, Bystryi RG, Norman GE, Pisarev VV, Stegailov VV. Molecular dynamics simulations of the relaxation processes in the condensed matter on GPUs. *Comput Phys Commun*. 2011;182(9):1974-1978. doi:10.1016/j.cpc.2010.12.026.

88. Nguyen TD, Phillips CL, Anderson JA, Glotzer SC. Rigid body constraints realized in massively-parallel molecular dynamics on graphics processing units. *Comput Phys Commun*. 2011;182(11):2307-2313. doi:10.1016/j.cpc.2011.06.005.

89. Howard MP, Anderson JA, Nikoubashman A, Glotzer SC, Panagiotopoulos AZ. Efficient neighbor list calculation for molecular simulation of colloidal systems using graphics processing units. *Comput Phys Commun*. 2016;203:45-52. doi:10.1016/j.cpc.2016.02.003.

90. Glaser J, Nguyen TD, Anderson JA, et al. Strong scaling of general-purpose molecular dynamics simulations on GPUs. *Comput Phys Commun*. 2015;192:97-107. doi:10.1016/j.cpc.2015.02.028.

91. Anderson JA, Eric Irrgang M, Glotzer SC. Scalable Metropolis Monte Carlo for simulation of hard shapes. *Comput Phys Commun*. 2016;204:21-30. doi:10.1016/j.cpc.2016.02.024.

92. Jiang L, Granick S. Real-Space, in Situ Maps of Hydrogel Pores. doi:10.1021/acsnano.6b04468.

93. Bryant SJ, Anseth KS. Hydrogel properties influence ECM production by chondrocytes photoencapsulated in poly(ethylene glycol) hydrogels. *J Biomed Mater Res*. 2002;59(1):63-72. doi:10.1002/jbm.1217.